Tseng, W., Penzien, J. "Soil-Foundation-Structure Interaction."
Bridge Engineering Handbook.
Ed. Wai-Fah Chen and Lian Duan
Boca Raton: CRC Press, 2000

42

Soil–Foundation–Structure Interaction

Wen-Shou Tseng
International Civil Engineering Consultants, Inc.

Joseph Penzien
International Civil Engineering Consultants, Inc.

42.1 Introduction

Prior to the 1971 San Fernando, California earthquake, nearly all damages to bridges during earthquakes were caused by ground failures, such as liquefaction, differential settlement, slides, and/or spreading; little damage was caused by seismically induced vibrations. Vibratory response considerations had been limited primarily to wind excitations of large bridges, the great importance of which was made apparent by failure of the Tacoma Narrows suspension bridge in the early 1940s, and to moving loads and impact excitations of smaller bridges.

The importance of designing bridges to withstand the vibratory response produced during earthquakes was revealed by the 1971 San Fernando earthquake during which many bridge structures collapsed. Similar bridge failures occurred during the 1989 Loma Prieta and 1994 Northridge, California earthquakes, and the 1995 Kobe, Japan earthquake. As a result of these experiences, much has been done recently to improve provisions in seismic design codes, advance modeling and analysis

procedures, and develop more effective detail designs, all aimed at ensuring that newly designed and retrofitted bridges will perform satisfactorily during future earthquakes.

Unfortunately, many of the existing older bridges in the United States and other countries, which are located in regions of moderate to high seismic intensity, have serious deficiencies which threaten life safety during future earthquakes. Because of this threat, aggressive actions have been taken in California, and elsewhere, to retrofit such unsafe bridges bringing their expected performances during future earthquakes to an acceptable level. To meet this goal, retrofit measures have been applied to the superstructures, piers, abutments, and foundations.

It is because of this most recent experience that the importance of coupled soil–foundation–structure interaction (SFSI) on the dynamic response of bridge structures during earthquakes has been fully realized. In treating this problem, two different methods have been used (1) the "elastodynamic" method developed and practiced in the nuclear power industry for large foundations and (2) the so-called empirical *p–y* method developed and practiced in the offshore oil industry for pile foundations. Each method has its own strong and weak characteristics, which generally are opposite to those of the other, thus restricting their proper use to different types of bridge foundation. By combining the models of these two methods in series form, a hybrid method is reported herein which makes use of the strong features of both methods, while minimizing their weak features. While this hybrid method may need some further development and validation at this time, it is fundamentally sound; thus, it is expected to become a standard procedure in treating seismic SFSI of large bridges supported on different types of foundation.

The subsequent sections of this chapter discuss all aspects of treating seismic SFSI by the elastodynamic, empirical *p–y*, and hybrid methods, including generating seismic inputs, characterizing soil–foundation systems, conducting force–deformation demand analyses using the substructuring approach, performing force–deformation capacity evaluations, and judging overall bridge performance.

42.2 Description of SFSI Problems

The broad problem of assessing the response of an engineered structure interacting with its supporting soil or rock medium (hereafter called soil medium for simplicity) under static and/or dynamic loadings will be referred here as the soil–structure interaction (SSI) problem. For a building that generally has its superstructure above ground fully integrated with its substructure below, reference to the SSI problem is appropriate when describing the problem of interaction between the complete system and its supporting soil medium. However, for a long bridge structure, consisting of a superstructure supported on multiple piers and abutments having independent and often distinct foundation systems which in turn are supported on the soil medium, the broader problem of assessing interaction in this case is more appropriately and descriptively referred to as the soil–foundation–structure interaction (SFSI) problem. For convenience, the SFSI problem can be separated into two subproblems, namely, a soil–foundation interaction (SFI) problem and a foundation–structure interaction (FSI) problem. Within the context of SFSI, the SFI part of the total problem is the one to be emphasized, since, once it is solved, the FSI part of the total problem can be solved following conventional structural response analysis procedures. Because the interaction between soil and the foundations of a bridge makes up the core of an SFSI problem, it is useful to review the different types of bridge foundations that may be encountered in dealing with this problem.

42.2.1 Bridge Foundation Types

From the perspective of SFSI, the foundation types commonly used for supporting bridge piers can be classified in accordance with their soil-support configurations into four general types: (1) spread footings, (2) caissons, (3) large-diameter shafts, and (4) slender-pile groups. These types as described separately below are shown in Figure 42.1.

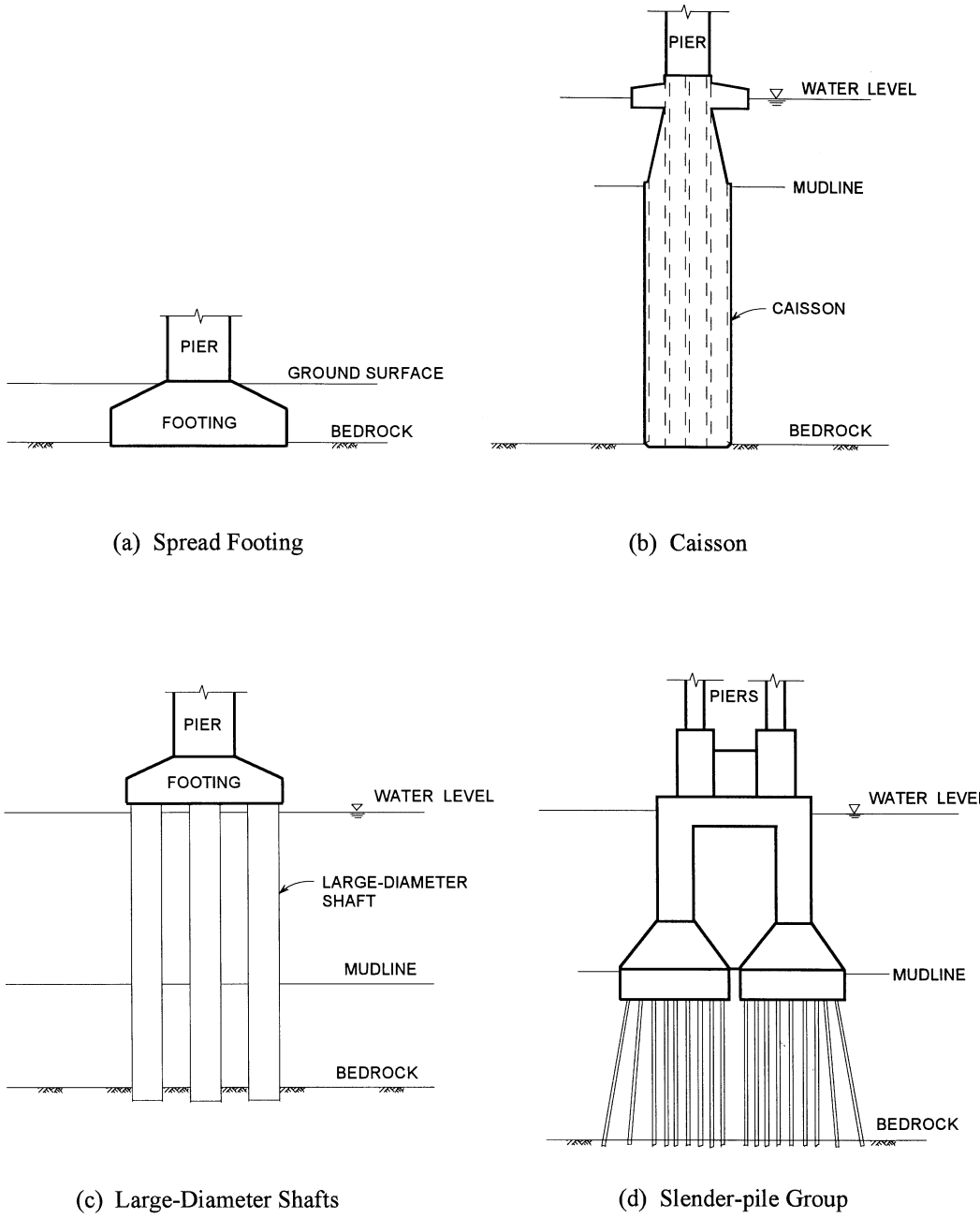

FIGURE 42.1 Bridge foundation types: (a) spread footing; (b) caisson; (c) large-diameter shafts; and (d) slender-pile group.

Spread Footings

Spread footings bearing directly on soil or rock are used to distribute the concentrated forces and moments in bridge piers and/or abutments over sufficient areas to allow the underlying soil strata to support such loads within allowable soil-bearing pressure limits. Of these loads, lateral forces are resisted by a combination of friction on the foundation bottom surface and passive soil pressure on its embedded vertical face. Spread footings are usually used on competent soils or rock which

have high allowable bearing pressures. These foundations may be of several forms, such as (1) isolated footings, each supporting a single column or wall pier; (2) combined footings, each supporting two or more closely spaced bridge columns; and (3) pedestals which are commonly used for supporting steel bridge columns where it is desirable to terminate the structural steel above grade for corrosion protection. Spread footings are generally designed to support the superimposed forces and moments without uplifting or sliding. As such, inelastic action of the soils supporting the footings is usually not significant.

Caissons

Caissons are large structural foundations, usually in water, that will permit dewatering to provide a dry condition for excavation and construction of the bridge foundations. They can take many forms to suit specific site conditions and can be constructed of reinforced concrete, steel, or composite steel and concrete. Most caissons are in the form of a large cellular rectangular box or cylindrical shell structure with a sealed base. They extend up from deep firm soil or rock-bearing strata to above mudline where they support the bridge piers. The cellular spaces within the caissons are usually flooded and filled with sand to some depth for greater stability. Caisson foundations are commonly used at deep-water sites having deep soft soils. Transfer of the imposed forces and moments from a single pier takes place by direct bearing of the caisson base on its supporting soil or rock stratum and by passive resistance of the side soils over the embedded vertical face of the caisson. Since the soil-bearing area and the structural rigidity of a caisson is very large, the transfer of forces from the caisson to the surrounding soil usually involves negligible inelastic action at the soil–caisson interface.

Large-Diameter Shafts

These foundations consist of one or more large-diameter, usually in the range of 4 to 12 ft (1.2 to 3.6 m), reinforced concrete cast-in-drilled-hole (CIDH) or concrete cast-in-steel-shell (CISS) piles. Such shafts are embedded in the soils to sufficient depths to reach firm soil strata or rock where a high degree of fixity can be achieved, thus allowing the forces and moments imposed on the shafts to be safely transferred to the embedment soils within allowable soil-bearing pressure limits and/or allowable foundation displacement limits. The development of large-diameter drilling equipment has made this type of foundation economically feasible; thus, its use has become increasingly popular. In actual applications, the shafts often extend above ground surface or mudline to form a single pier or a multiple-shaft pier foundation. Because of their larger expected lateral displacements as compared with those of a large caisson, a moderate level of local soil nonlinearities is expected to occur at the soil–shaft interfaces, especially near the ground surface or mudline. Such nonlinearities may have to be considered in design.

Slender-Pile Groups

Slender piles refer to those piles having a diameter or cross-sectional dimensions less than 2 ft (0.6 m). These piles are usually installed in a group and provided with a rigid cap to form the foundation of a bridge pier. Piles are used to extend the supporting foundations (pile caps) of a bridge down through poor soils to more competent soil or rock. The resistance of a pile to a vertical load may be essentially by point bearing when it is placed through very poor soils to a firm soil stratum or rock, or by friction in case of piles that do not achieve point bearing. In real situations, the vertical resistance is usually achieved by a combination of point bearing and side friction. Resistance to lateral loads is achieved by a combination of soil passive pressure on the pile cap, soil resistance around the piles, and flexural resistance of the piles. The uplift capacity of a pile is generally governed by the soil friction or cohesion acting on the perimeter of the pile. Piles may be installed by driving or by casting in drilled holes. Driven piles may be timber piles, concrete piles with or without prestress, steel piles in the form of pipe sections, or steel piles in the form of structural shapes (e.g., H shape). Cast-in-drilled-hole piles are reinforced concrete piles installed with or without steel casings. Because of their relatively small cross-sectional dimensions, soil resistance to large pile loads usually develops large local soil nonlinearities that must

be considered in design. Furthermore, since slender piles are normally installed in a group, mutual interactions among piles will reduce overall group stiffness and capacity. The amounts of these reductions depend on the pile-to-pile spacing and the degree ofsoil nonlinearity developed in resisting the loads.

42.2.2 Definition of SFSI Problem

For a bridge subjected to externally applied static and/or dynamic loadings on the aboveground portion of the structure, the SFSI problem involves evaluation of the structural performance (demand/capacity ratio) of the bridge under the applied loadings taking into account the effect of SFI. Since in this case the ground has no initial motion prior to loading, the effect of SFI is to provide the foundation–structure system with a flexible boundary condition at the soil–foundation interface location when static loading is applied and a compliant boundary condition when dynamic loading is applied. The SFI problem in this case therefore involves (1) evaluation of the soil–foundation interface boundary flexibility or compliance conditions for each bridge foundation, (2) determination of the effects of these boundary conditions on the overall structural response of the bridge (e.g., force, moment, or deformation) demands, and (3) evaluation of the resistance capacity of each soil–foundation system that can be compared with the corresponding response demand in assessing performance. That part of determining the soil–foundation interface boundary flexibilities or compliances will be referred to subsequently in a gross term as the "foundation stiffness or impedance problem"; that part of determining the structural response of the bridge as affected by the soil–foundation boundary flexibilities or compliances will be referred to as the "foundation–structure interaction problem"; and that part of determining the resistance capacity of the soil–foundation system will be referred to as the "foundation capacity problem."

For a bridge structure subjected to seismic conditions, dynamic loadings are imposed on the structure. These loadings, which originate with motions of the soil medium, are transmitted to the structure through its foundations; therefore, the overall SFSI problem in this case involves, in addition to the foundation impedance, FSI, and foundation capacity problems described above, the evaluation of (1) the soil forces acting on the foundations as induced by the seismic ground motions, referred to subsequently as the "seismic driving forces," and (2) the effects of the free-field ground-motion-induced soil deformations on the soil–foundation boundary compliances and on the capacity of the soil–foundation systems. In order to evaluate the seismic driving forces on the foundations and the effects of the free-field ground deformations on compliances and capacities of the soil–foundation systems, it is necessary to determine the variations of free-field motion within the ground regions which interact with the foundations. This problem of determining the free-field ground motion variations will be referred to herein as the "free-field site response problem." As will be shown later, the problem of evaluating the seismic driving forces on the foundations is equivalent to determining the "effective or scattered foundation input motions" induced by the free-field soil motions. This problem will be referred to here as the "foundation scattering problem."

Thus, the overall SFSI problem for a bridge subjected to externally applied static and/or dynamic loadings can be separated into the evaluation of (1) foundation stiffnesses or impedances, (2) foundation–structure interactions, and (3) foundation capacities. For a bridge subjected to seismic ground motion excitations, the SFSI problem involves two additional steps, namely, the evaluation of free-field site response and foundation scattering. When solving the total SFSI problem, the effects of the nonzero soil deformation state induced by the free-field seismic ground motions should be evaluated in all five steps mentioned above.

42.2.3 Demand vs. Capacity Evaluations

As described previously, assessing the seismic performance of a bridge system requires evaluation of SFSI involving two parts. One part is the evaluation of the effects of SFSI on the seismic-response demands within the system; the other part is the evaluation of the seismic force and/or deformation

capacities within the system. Ideally, a well-developed methodology should be one that is capable of solving these two parts of the problem concurrently in one step using a unified suitable model for the system. Unfortunately, to date, such a unified method has not yet been developed. Because of the complexities of a real problem and the different emphases usually demanded of the solutions for the two parts, different solution strategies and methods of analysis are warranted for solving these two parts of the overall SFSI problem. To be more specific, evaluation on the demand side of the problem is concerned with the overall SFSI system behavior which is controlled by the mass, damping (energy dissipation), and stiffness properties, or, collectively, the impedance properties, of the entire system; and, the solution must satisfy the dynamic equilibrium and compatibility conditions of the global system. This system behavior is not sensitive, however, to approximations made on local element behavior; thus, its evaluation does not require sophisticated characterizations of the detailed constitutive relations of its local elements. For this reason, evaluation of demand has often been carried out using a linear or equivalent linear analysis procedure. On the contrary, evaluation of capacity must be concerned with the extreme behavior of local elements or subsystems; therefore, it must place emphasis on the detailed constitutive behaviors of the local elements or subsystems when deformed up to near-failure levels. Since only local behaviors are of concern, the evaluation does not have to satisfy the global equilibrium and compatibility conditions of the system fully. For this reason, evaluation of capacity is often obtained by conducting nonlinear analyses of detailed local models of elements or subsystems or by testing of local members, connections, or sub-assemblages, subjected to simple pseudo-static loading conditions.

Because of the distinct differences between effective demand and capacity analyses as described above, the analysis procedures presented subsequently differentiate between these two parts of the overall SFSI problem.

42.3 Current State-of-the-Practice

The evaluation of SFSI effects on bridges located in regions of high seismicity has not received as much attention as for other critical engineered structures, such as dams, nuclear facilities, and offshore structures. In the past, the evaluation of SFSI effects for bridges has, in most cases, been regarded as a part of the bridge foundation design problem. As such, emphasis has been placed on the evaluation of load-resisting capacities of various foundation systems with relatively little attention having been given to the evaluation of SFSI effects on seismic-response demands within the complete bridge system. Only recently has formal SSI analysis methodologies and procedures, developed and applied in other industries, been adopted and applied to seismic performance evaluations of bridges [1], especially large important bridges [2,3].

Even though the SFSI problems for bridges pose their own distinct features (e.g., multiple independent foundations of different types supported in highly variable soil conditions ranging from hard to very soft), the current practice is to adopt, with minor modifications, the same methodologies and procedures developed and practiced in other industries, most notably, the nuclear power and offshore oil industries. Depending upon the foundation type and its soil-support condition, the procedures currently being used in evaluating SFSI effects on bridges can broadly be classified into two main methods, namely, the so-called elastodynamic method that has been developed and practiced in the nuclear power industry for large foundations, and the so-called empirical p–y method that has been developed and practiced in the offshore oil industry for pile foundations. The bases and applicabilities of these two methods are described separately below.

42.3.1 Elastodynamic Method

This method is based on the well-established elastodynamic theory of wave propagation in a linear elastic, viscoelastic, or constant-hysteresis-damped elastic half-space soil medium. The fundamental element of this method is the constitutive relation between an applied harmonic point load and

the corresponding dynamic response displacements within the medium called the dynamic Green's functions. Since these functions apply only to a linear elastic, visoelastic, or constant-hysteresis-damped elastic medium, they are valid only for linear SFSI problems. Since application of the elastodynamic method of analysis uses only mass, stiffness, and damping properties of an SFSI system, this method is suitable only for global system response analysis applications. However, by adopting the same equivalent linearization procedure as that used in the seismic analysis of free-field soil response, e.g., that used in the computer program SHAKE [4], the method has been extended to one that can accommodate global soil nonlinearities, i.e., those nonlinearities induced in the free-field soil medium by the free-field seismic waves [5].

Application of the elastodynamic theory to dynamic SFSI started with the need for solving machine–foundation vibration problems [6]. Along with other rapid advances in earthquake engineering in the 1970s, application of this theory was extended to solving seismic SSI problems for building structures, especially those of nuclear power plants [7–9]. Such applications were enhanced by concurrent advances in analysis techniques for treating soil dynamics, including development of the complex modulus representation of dynamic soil properties and use of the equivalent linearization technique for treating ground-motion-induced soil nonlinearities [10–12]. These developments were further enhanced by the extensive model calibration and methodology validation and refinement efforts carried out in a comprehensive large-scale SSI field experimental program undertaken by the Electric Power Research Institute (EPRI) in the 1980s [13]. All of these efforts contributed to advancing the elastodynamic method of SSI analysis currently being practiced in the nuclear power industry [5].

Because the elastodynamic method of analysis is capable of incorporating mass, stiffness, and damping characteristics of each soil, foundation, and structure subsystem of the overall SFSI system, it is capable of capturing the dynamic interactions between the soil and foundation subsystems and between the foundations and structure subsystem; thus, it is suitable for seismic demand analyses. However, since the method does not explicitly incorporate strength characteristics of the SFSI system, it is not suitable for capacity evaluations.

As previously mentioned in Section 42.2.1, there are four types of foundation commonly used for bridges: (1) spread footings, (2) caissons, (3) large-diameter shafts, and (4) slender-pile groups. Since only small local soil nonlinearities are induced at the soil–foundation interfaces of spread footings and caissons, application of the elastodynamic method of seismic demand analysis of the complete SFSI system is valid. However, the validity of applying this method to large-diameter shaft foundations depends on the diameter of the shafts and on the amplitude of the imposed loadings. When the shaft diameter is large so that the load amplitudes produce only small local soil nonlinearities, the method is reasonably valid. However, when the shaft diameter is relatively small, the larger-amplitude loadings will produce local soil nonlinearities sufficiently large to require that the method be modified as discussed subsequently. Application of the elastodynamic method to slender-pile groups is usually invalid because of the large local soil nonlinearities which develop near the pile boundaries. Only for very low amplitude loadings can the method be used for such foundations.

42.3.2 Empirical "*p-y*" Method

This method was originally developed for the evaluation of pile–foundation response due to lateral loads [14–16] applied externally to offshore structures. As used, it characterizes the lateral soil resistance per unit length of pile, p, as a function of the lateral displacement, y. The p–y relation is generally developed on the basis of an empirical curve which reflects the nonlinear resistance of the local soil surrounding the pile at a specified depth (Figure 42.2). Construction of the curve depends mainly on soil material strength parameters, e.g., the friction angle, ϕ, for sands and cohesion, c, for clays at the specified depth. For shallow soil depths where soil surface effects become important, construction of these curves also depends on the local soil failure mechanisms, such as failure by a passive soil resistance wedge. Typical p–y curves developed for a pile at different soil depths are shown in Figure 42.3. Once the set of p–y curves representing the soil resistances at discrete values

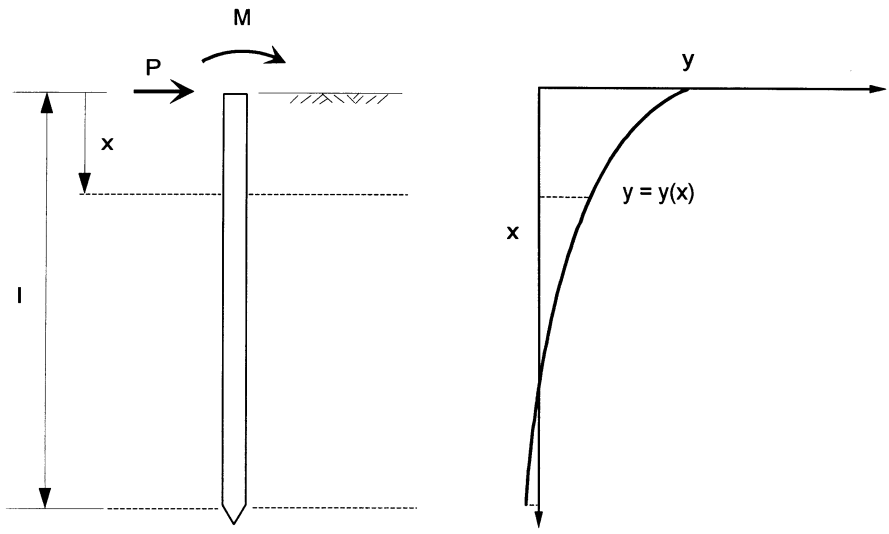

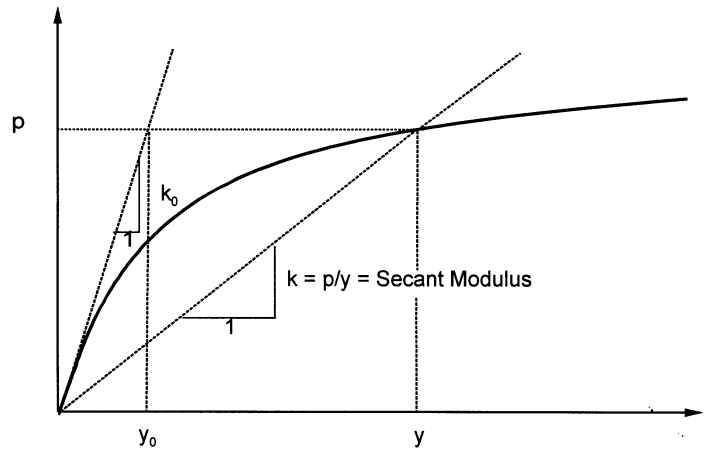

FIGURE 42.2 Empirical *p–y* curves and secant modulus.

of depth along the length of the pile has been constructed, evaluation of pile response under a specified set of lateral loads is accomplished by solving the problem of a beam supported laterally on discrete nonlinear springs. The validity and applicability of this method are based on model calibrations and correlations with field experimental results [15,16].

Based on the same model considerations used in developing the *p–y* curves for lateral response analysis of piles, the method has been extended to treating the axial resistance of soils to piles per unit length of pile, *t*, as a nonlinear function of the corresponding axial displacement, z, resulting in the so-called axial *t–z* curve, and treating the axial resistance of the soils at the pile tip, *Q*, as a

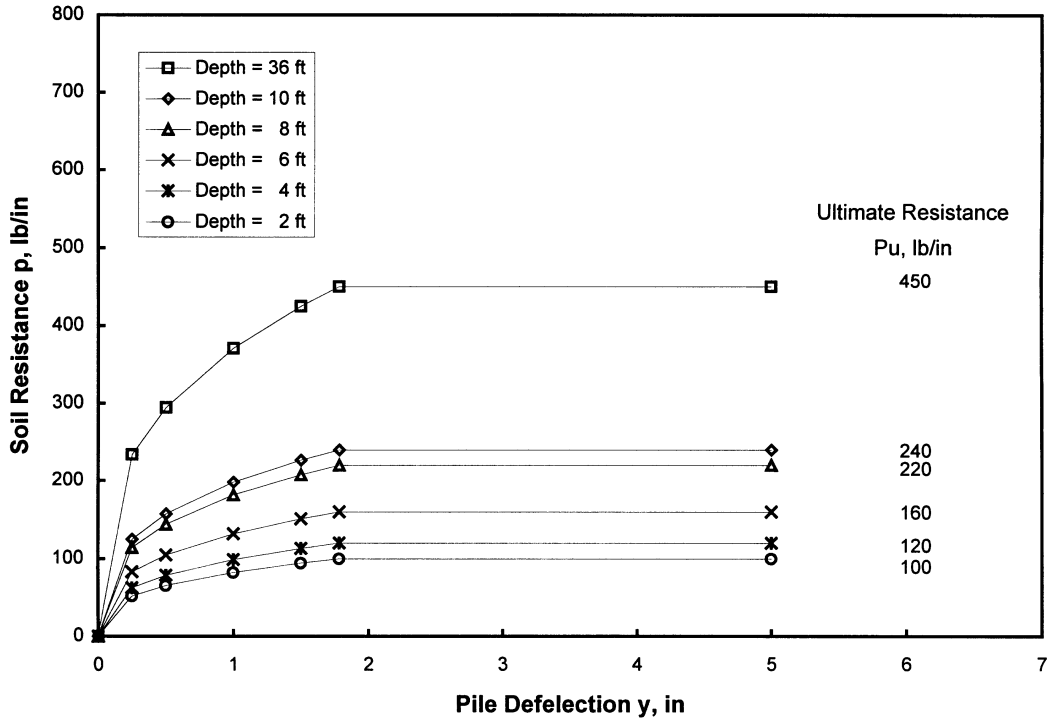

FIGURE 42.3 Typical *p–y* curves for a pile at different depths.

nonlinear function of the pile tip axial displacement, *d*, resulting in the so-called *Q–d* curve. Again, the construction of the *t–z* and *Q–d* curves for a soil-supported pile is based on empirical curvilinear forms and the soil strength parameters as functions of depth. By utilizing the set of *p–y*, *t–z*, and *Q–d* curves developed for a pile foundation, the response of the pile subjected to general three-dimensional (3-D) loadings applied at the pile head can be solved using the model of a 3-D beam supported on discrete sets of nonlinear lateral *p–y*, axial *t–z*, and axial *Q–d* springs. The method as described above for solving a soil-supported pile foundation subjected to applied loadings at the pile head is referred to here as the empirical *p–y* method, even though it involves not just the lateral *p–y* curves but also the axial *t–z* and *Q–d* curves for characterizing the soil resistances.

Since this method depends primarily on soil-resistance strength parameters and does not incorporate soil mass, stiffness, and damping characteristics, it is, strictly speaking, only applicable for capacity evaluations of slender-pile foundations and is not suitable for seismic demand evaluations because, as mentioned previously, a demand evaluation for an SFSI system requires the incorporation of the mass, stiffness, and damping properties of each of the constituent parts, namely, the soil, foundation, and structure subsystems.

Even though the *p–y* method is not strictly suited to demand analyses, it is current practice in performing seismic-demand evaluations for bridges supported on slender-pile group foundations to make use of the empirical nonlinear *p–y*, *t–z*, and *Q–d* curves in developing a set of equivalent linear lateral and axial soil springs attached to each pile at discrete elevations in the foundation. The soil–pile systems developed in this manner are then coupled with the remaining bridge structure to form the complete SFSI system for use in a seismic demand analysis. The initial stiffnesses of the equivalent linear *p–y*, *t–z*, and *Q–d* soil springs are based on secant moduli of the nonlinear *p–y*, *t–y*, and *Q–d* curves, respectively, at preselected levels of lateral and axial pile displacements, as shown schematically in Figure 42.2. After completing the initial demand analysis, the amplitudes of pile displacement are compared with the corresponding preselected amplitudes to check on their

mutual compatibilities. If incompatibilities exist, the initial set of equivalent linear stiffnesses is adjusted and a second demand analysis is performed. Such iterations continue until reasonable compatibility is achieved. Since soil inertia and damping properties are not included in the above-described demand analysis procedure, it must be considered approximate; however, it is reasonably valid when the nonlinearities in the soil resistances become so large that the inelastic components of soil deformations adjacent to piles are much larger than the corresponding elastic components. This condition is true for a slender-pile group foundation subjected to relatively large amplitude pile-head displacements. However, for a large-diameter shaft foundation, having larger soil-bearing areas and higher shaft stiffnesses, the inelastic components of soil deformations may be of the same order or even smaller than the elastic components, in which case, application of the empirical p–y method for a demand analysis as described previously can result in substantial errors.

42.4 Seismic Inputs to SFSI System

The first step in conducting a seismic performance evaluation of a bridge structure is to define the seismic input to the coupled soil–foundation–structure system. In a design situation, this input is defined in terms of the expected free-field motions in the soil region surrounding each bridge foundation. It is evident that to characterize such motions precisely is practically unachievable within the present state of knowledge of seismic ground motions. Therefore, it is necessary to use a rather simplistic approach in generating such motions for design purposes. The procedure most commonly used for designing a large bridge is to (1) generate a three-component (two horizontal and vertical) set of accelerograms representing the free-field ground motion at a "control point" selected for the bridge site and (2) characterize the spatial variations of the free-field motions within each soil region of interest relative to the control motions.

The control point is usually selected at the surface of bedrock (or surface of a firm soil stratum in case of a deep soil site), referred to here as "rock outcrop," at the location of a selected reference pier; and the free-field seismic wave environment within the local soil region of each foundation is assumed to be composed of vertically propagating plane shear (S) waves for the horizontal motions and vertically propagating plane compression (P) waves for the vertical motions. For a bridge site consisting of relatively soft topsoil deposits overlying competent soil strata or rock, the assumption of vertically propagating plane waves over the depth of the foundations is reasonably valid as confirmed by actual field downhole array recordings [17].

The design ground motion for a bridge is normally specified in terms of a set of parameter values developed for the selected control point which include a set of target acceleration response spectra (ARS) and a set of associated ground motion parameters for the design earthquake, namely (1) magnitude, (2) source-to-site distance, (3) peak ground (rock-outcrop) acceleration (PGA), velocity (PGV), and displacement (PGD), and (4) duration of strong shaking. For large important bridges, these parameter values are usually established through regional seismic investigations coupled with site-specific seismic hazard and ground motion studies, whereas, for small bridges, it is customary to establish these values based on generic seismic study results such as contours of regional PGA values and standard ARS curves for different general classes of site soil conditions.

For a long bridge supported on multiple piers which are in turn supported on multiple foundations spaced relatively far apart, the spatial variations of ground motions among the local soil regions of the foundations need also be defined in the seismic input. Based on the results of analyses using actual earthquake ground motion recordings obtained from strong motion instrument arrays, such as the El Centro differential array in California and the SMART-1 array in Taiwan, the spatial variations of free-field seismic motions have been characterized using two parameters: (1) apparent horizontal wave propagation velocity (speed and direction) which controls the first-order spatial variations of ground motion due to the seismic wave passage effect and (2) a set of horizontal and vertical ground motion "coherency functions" which quantifies the second-order ground motion variations due to scattering and complex 3-D wave propagation [18]. Thus, in addition to the design

ground motion parameter values specified for the control motion, characterizing the design seismic inputs to long bridges needs to include the two additional parameters mentioned above, namely, (1) apparent horizontal wave velocity and (2) ground motion coherency functions; therefore, the seismic input motions developed for the various pier foundation locations need to be compatible with the values specified for these two additional parameters.

Having specified the design seismic ground motion parameters, the steps required in establishing the pier foundation location-specific seismic input motions for a particular bridge are

1. Develop a three-component (two horizontal and vertical) set of free-field rock-outcrop motion time histories which are compatible with the design target ARS and associated design ground motion parameters applicable at a selected single control point location at the bridge site (these motions are referred to here simply as the "response spectrum compatible time histories" of control motion).
2. Generate response-spectrum-compatible time histories of free-field rock-outcrop motions at each bridge pier support location such that their coherencies relative to the corresponding components of the response spectrum compatible motions at the control point and at other pier support locations are compatible with the wave passage parameters and the coherency functions specified for the site (these motions are referred to here as "response spectrum and coherency compatible motions).
3. Carry out free-field site response analyses for each pier support location to obtain the time-histories of free-field soil motions at specified discrete elevations over the full depth of each foundation using the corresponding response spectrum and coherency compatible free-field rock-outcrop motions as inputs.

In the following sections, procedures will be presented for generating the set of response spectrum compatible rock-outcrop time histories of motion at the control point location and for generating the sets of response spectrum and coherency compatible rock-outcrop time histories of motion at all pier support locations, and guidelines will be given for performing free-field site response analyses.

42.4.1 Free-Field Rock-Outcrop Motions at Control-Point Location

Given a prescribed set of target ARS and a set of associated design ground motion parameters for a bridge site as described previously, the objective here is to develop a three-component set of time histories of control motion that (1) provides a reasonable match to the corresponding target ARS and (2) has time history characteristics reasonably compatible with the other specified associated ground motion parameter values. In the past, several different procedures have been used for developing rock-outcrop time histories of motion compatible with a prescribed set of target ARS. These procedures are summarized as follows:

1. *Response Spectrum Compatibility Time History Adjustment Method* [19–22] — This method as generally practiced starts by selecting a suitable three-component set of initial or "starting" accelerograms and proceeds to adjust each of them iteratively, using either a time-domain [21,23] or a frequency-domain [19,20,22] procedure, to achieve compatibility with the specified target ARS and other associated parameter values. The time-domain adjustment procedure usually produces only small local adjustments to the selected starting time histories, thereby producing response spectrum compatible time histories closely resembling the initial motions. The general "phasing" of the seismic waves in the starting time history is largely maintained while achieving close compatibility with the target ARS: minor changes do occur, however, in the phase relationships. The frequency-domain procedure as commonly used retains the phase relationships of an initial motion, but does not always provide as close a fit to the target spectrum as does the time-domain procedure. Also, the motion produced by the frequency-domain procedure shows greater visual differences from the initial motion.

2. *Source-to-Site Numerical Model Time History Simulation Method* [24–27] — This method generally starts by constructing a numerical model to represent the controlling earthquake source and source-to-site transmission and scattering functions, and then accelerograms are synthesized for the site using numerical simulations based on various plausible fault-rupture scenarios. Because of the large number of time history simulations required in order to achieve a "stable" average ARS for the ensemble, this method is generally not practical for developing a complete set of time histories to be used directly; rather it is generally used to supplement a set of actual recorded accelerograms, in developing site-specific target response spectra and associated ground motion parameter values.
3. *Multiple Actual Recorded Time History Scaling Method* [28,29] — This method starts by selecting multiple 3-component sets (generally ≥7) of actual recorded accelerograms which are subsequently scaled in such a way that the average of their response spectral ordinates over the specified frequency (or period) range of interest matches the target ARS. Experience in applying this method shows that its success depends very much on the selection of time histories. Because of the lack of suitable recorded time histories, individual accelerograms often have to be scaled up or down by large multiplication factors, thus raising questions about the appropriateness of such scaling. Experience also indicates that unless a large ensemble of time histories (typically >20) are selected, it is generally difficult to achieve matching of the target ARS over the entire spectral frequency (or period) range of interest.
4. *Connecting Accelerogram Segments Method* [55] — This method produces a synthetic time history by connecting together segments of a number of actual recorded accelerograms in such a way that the ARS of the resulting time history fits the target ARS reasonably well. It generally requires producing a number of synthetic time histories to achieve acceptable matching of the target spectrum over the entire frequency (or period) range of interest.

At the present time, Method 1 is considered most suitable and practical for bridge engineering applications. In particular, the time-domain time history adjustment procedure which produces only local time history disturbances has been applied widely in recent applications. This method as developed by Lilhanand and Tseng [21] in 1988, which is based on earlier work by Kaul [30] in 1978, is described below.

The time-domain procedure for time history adjustment is based on the inherent definition of a response spectrum and the recognition that the times of occurrence of the response spectral values for the specified discrete frequencies and damping values are not significantly altered by adjustments of the time history in the neighborhoods of these times. Thus, each adjustment, which is made by adding a small perturbation, $\delta a(t)$, to the selected initial or starting acceleration time history, $a(t)$, is carried out in an iterative manner such that, for each iteration, i, an adjusted acceleration time history, $a_i(t)$, is obtained from the previous acceleration time history, $a_{(i\text{-}1)}(t)$, using the relation

$$a_i(t) = a_{(i\text{-}1)}(t) + \delta a_i(t) \tag{42.1}$$

The small local adjustment, $\delta a_i(t)$, is determined by solving the integral equation

$$\delta Ri(\omega_j, \beta_k) = \int_0^{t_{jk}} \delta a_i(\tau) h_{jk}(t_{jk} - \tau) d\tau \tag{42.2}$$

which expresses the small change in the acceleration response value $\delta R_i(\omega_j, \beta_k)$ for frequency ω_j and damping β_k resulting from the local time history adjustment $\delta a_i(t)$. This equation makes use of the acceleration unit–impulse response function $h_{jk}(t)$ for a single-degree-of-freedom oscillator having a natural frequency ω_j and a damping ratio β_k. Quantity t_{jk} in the integral represents the time at which its corresponding spectral value occurs, and τ is a time lag.

By expressing $\delta a_i(t)$ as a linear combination of impulse response functions with unknown coefficients, the above integral equation can be transformed into a system of linear algebraic equations that can easily be solved for the unknown coefficients. Since the unit–impulse response functions decay rapidly due to damping, they produce only localized perturbations on the acceleration time history. By repeatedly applying the above adjustment, the desired degree of matching between the response spectra of the modified motions and the corresponding target spectra is achieved, while, in doing so, the general characteristics of the starting time history selected for adjustment are preserved.

Since this method of time history modification produces only local disturbances to the starting time history, the time history phasing characteristics (wave sequence or pattern) in the starting time history are largely maintained. It is therefore important that the starting time history be selected carefully. Each three-component set of starting accelerograms for a given bridge site should preferably be a set recorded during a past seismic event that has (1) a source mechanism similar to that of the controlling design earthquake, (2) a magnitude within about ±0.5 of the target controlling earthquake magnitude, and (3) a closest source-to-site distance within 10 km of the target source-to-site distance. The selected recorded accelerograms should have their PGA, PGV, and PGD values and their strong shaking durations within a range of ±25% of the target values specified for the bridge site and they should represent free-field surface recordings on rock, rocklike, or a stiff soil site; no recordings on a soft site should be used. For a close-in controlling seismic event, e.g., within about 10 km of the site, the selected accelerograms should contain a definite velocity pulse or the so-called fling. When such recordings are not available, Method 2 described previously can be used to generate a starting set of time histories having an appropriate fling or to modify the starting set of recorded motions to include the desired directional velocity pulse.

Having selected a three-component set of starting time histories, the horizontal components should be transformed into their principal components and the corresponding principal directions should be evaluated [31]. These principal components should then be made response spectrum compatible using the time-domain adjustment procedure described above or the standard frequency-domain adjustment procedure[20,22,32]. Using the latter procedure, only the Fourier amplitude spectrum, not the phase spectrum, is adjusted iteratively.

The target acceleration response spectra are in general identical for the two horizontal principal components of motion; however, a distinct target spectrum is specified for the vertical component. In such cases, the adjusted response spectrum compatible horizontal components can be oriented horizontally along any two orthogonal coordinate axes in the horizontal plane considered suitable for structural analysis applications. However, for bridge projects that have controlling seismic events with close-in seismic sources, the two horizontal target response spectra representing motions along a specified set of orthogonal axes are somewhat different, especially in the low-frequency (long-period) range; thus, the response spectrum compatible time histories must have the same definitive orientation. In this case, the generated three-component set of response spectrum compatible time histories should be used in conjunction with their orientation. The application of this three-component set of motions in a different coordinate orientation requires transforming the motions to the new coordinate system. It should be noted that such a transformation of the components will generally result in time histories that are not fully compatible with the original target response spectra. Thus, if response spectrum compatibility is desired in a specific coordinate orientation (such as in the longitudinal and transverse directions of the bridge), target response spectra in the specific orientation should be generated first and then a three-component set of fully response spectrum compatible time histories should be generated for this specific coordinate system.

As an example, a three-component set of response spectrum compatible time histories of control motion, generated using the time-domain time history adjustment procedure, is shown in Figure 42.4.

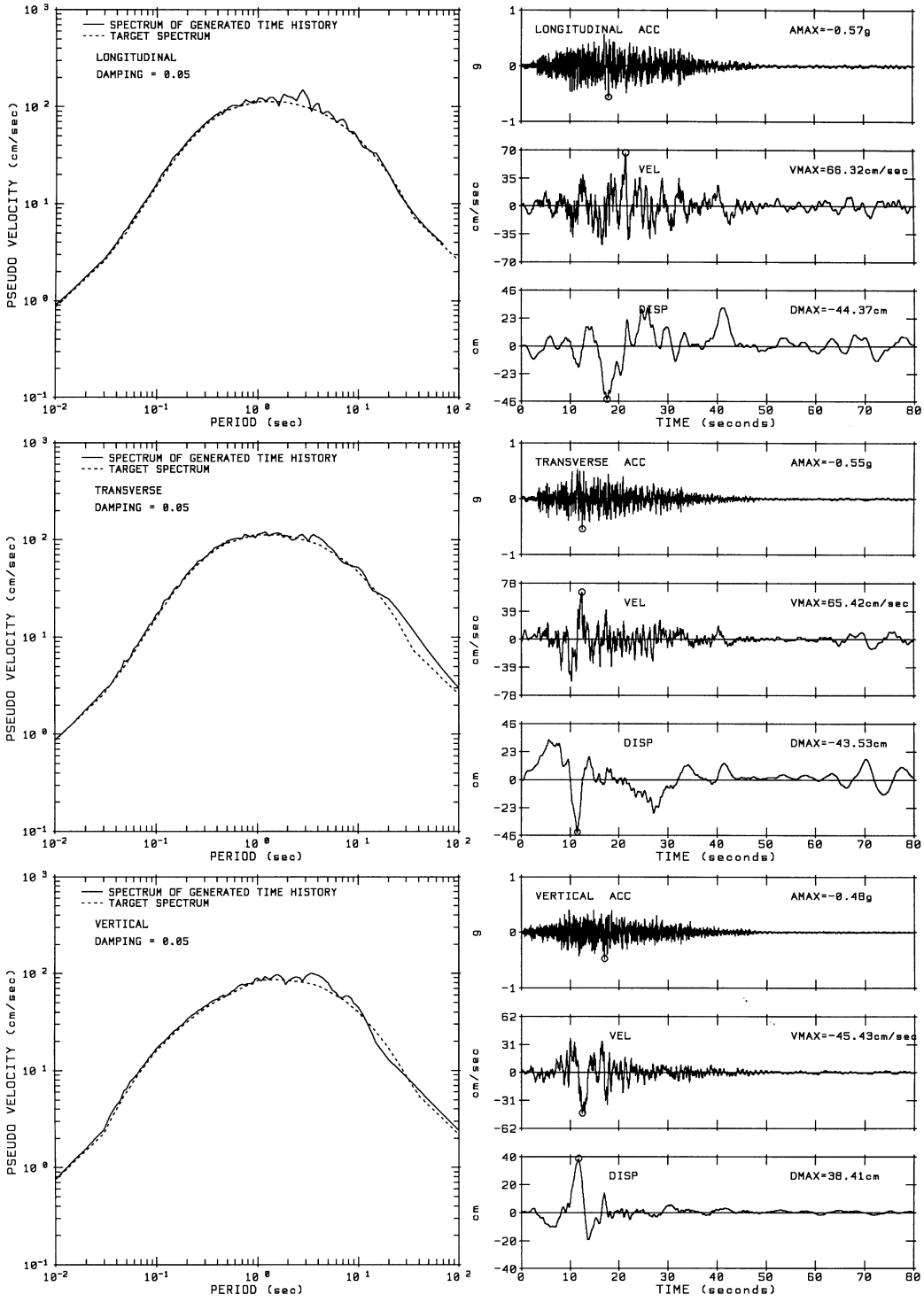

FIGURE 42.4 Examples of a three-component set of response spectrum compatible time histories of control motion.

42.4.2 Free-Field Rock-Outcrop Motions at Bridge Pier Support Locations

As mentioned previously, characterization of the spatial variations of ground motions for engineering purposes is based on a set of wave passage parameters and ground motion coherency functions. The wave passage parameters currently used are the apparent horizontal seismic wave speed, V, and its direction angle θ relative to an axis normal to the longitudinal axis of the bridge. Studies of strong- and weak-motion array data including those in California, Taiwan, and Japan show that the apparent horizontal speed of S-waves in the direction of propagation is typically in the 2 to 3 km/s range [18,33]. In applications, the apparent wave-velocity vector showing speed and direction must be projected along the bridge axis giving the apparent wave speed in that direction as expressed by

$$V_{\text{bridge}} = \frac{V}{\sin\theta} \tag{42.3}$$

To be realistic, when θ becomes small, a minimum angle for θ, say, 30°, should be used in order to account for waves arriving in directions different from the specified direction.

The spatial coherency of the free-field components of motion in a single direction at various locations on the ground surface has been parameterized by a complex coherency function defined by the relation

$$\Gamma_{ij}(i\omega) = \frac{S_{ij}(i\omega)}{\sqrt{S_{ii}(\omega)}\sqrt{S_{jj}(\omega)}} \qquad i, j = 1, 2, \ldots, n \text{ locations} \tag{42.4}$$

in which $S_{ij}(i\omega)$ is the smoothed complex cross-power spectral density function and $S_{ii}(\omega)$ and $S_{jj}(\omega)$ are the smoothed real power spectral density (PSD) functions of the components of motion at locations i and j. The notation $i\omega$ in the above equation is used to indicate that the coefficients $S_{ij}(i\omega)$ are complex valued (contain both real and imaginary parts) and are dependent upon excitation frequency ω. Based on analyses of strong-motion array data, a set of generic coherency functions for the horizontal and vertical ground motions has been developed [34]. These functions for discrete separation distances between locations i and j are plotted against frequency in Figure 42.5.

Given a three-component set of response spectrum compatible time histories of rock-outcrop motions developed for the selected control point location and a specified set of wave passage parameters and "target" coherency functions as described above, response spectrum compatible and coherency compatible multiple-support rock-outcrop motions applicable to each pier support location of the bridge can be generated using the procedure presented below. This procedure is based on the "marching method" developed by Hao et al. [32] in 1989 and extended by Tseng et al. [35] in 1993.

Neglecting, for the time being, ground motion attenuation along the bridge axis, the components of rock-outcrop motions at all pier support locations in a specific direction have PSD functions which are common with the PSD function $S_o(\omega)$ specified for the control motion, i.e.,

$$S_{ii}(\omega) = S_{jj}(\omega) = S_o(\omega) = |u_o(i\omega)|^2 \tag{42.5}$$

where $u_o(i\omega)$ is the Fourier transform of the corresponding component of control motion, $u_o(t)$. By substituting Eq. (42.5) into Eq. (42.4), one obtains

$$S_{ij}(i\omega) = \Gamma_{ij}(i\omega)\, S_o(\omega) \tag{42.6}$$

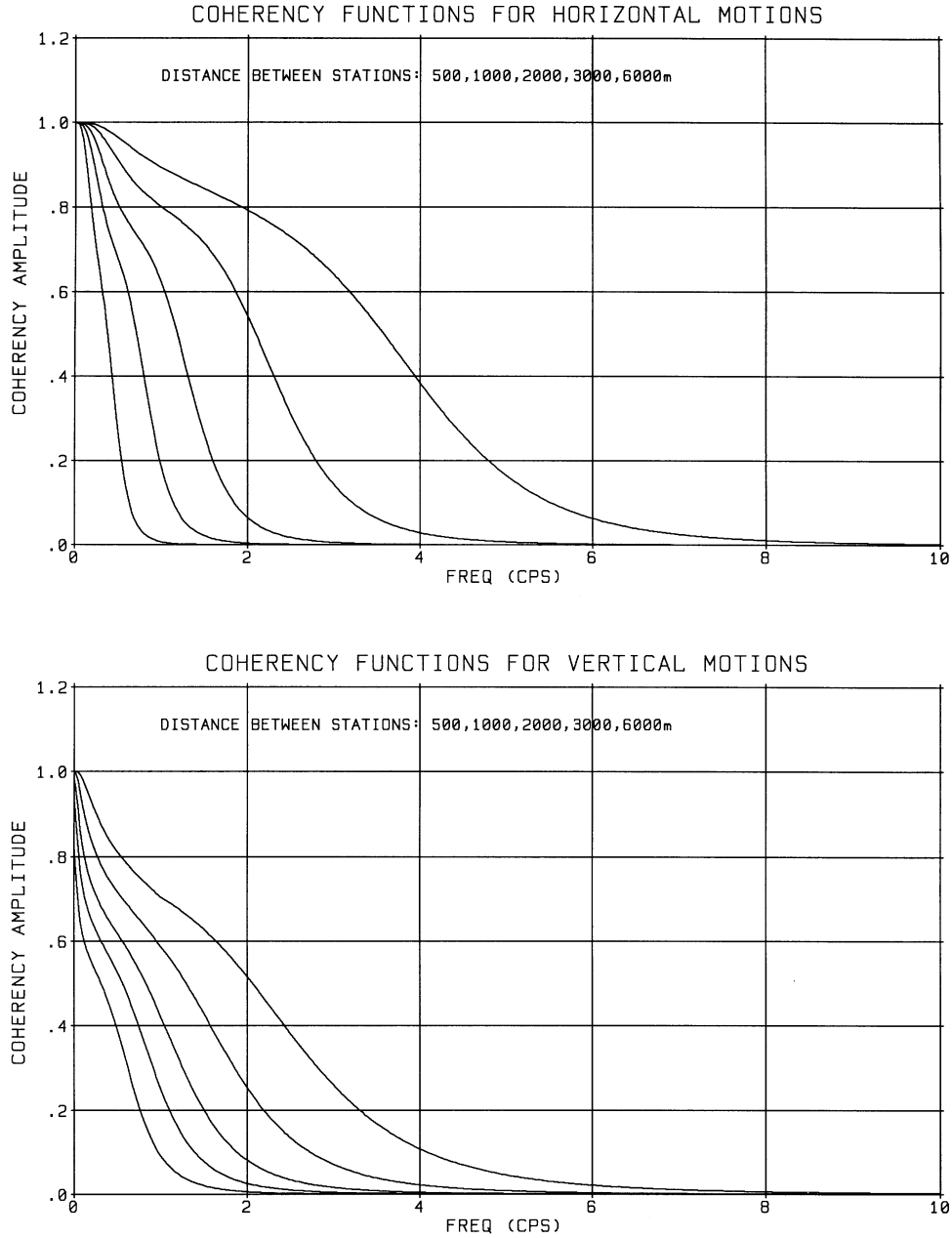

FIGURE 42.5 Example of coherency functions of frequency at discrete separation distances.

which can be rewritten in a matrix form for all pier support locations as follows:

$$\boldsymbol{S}(i\omega) = \boldsymbol{\Gamma}(i\omega)\, S_o(\omega) \tag{42.7}$$

Since, by definition, the coherency matrix $\boldsymbol{\Gamma}(i\omega)$ is an Hermitian matrix, it can be decomposed into a complex conjugate pair of lower and upper triangular matrices $\boldsymbol{L}(i\omega)$ and $\boldsymbol{L}^*(i\omega)^T$ as expressed by

$$\boldsymbol{\Gamma}(i\omega) = \boldsymbol{L}(i\omega)\ \ \boldsymbol{L}^*(i\omega)^T \tag{42.8}$$

in which the symbol * denotes complex conjugate. In proceeding, let

$$\boldsymbol{u}(i\omega) = \boldsymbol{L}(i\omega)\boldsymbol{\eta}_{\phi_i}(i\omega)u_o(i\omega) \tag{42.9}$$

in which $\boldsymbol{u}(\omega)$ is a vector containing components of motion $u_i(\omega)$ for locations, $i = 1, 2, \ldots, n$; and, $\boldsymbol{\eta}_{\phi_i}(i\omega) = \{e^{i\phi_i(\omega)}\}$ is a vector containing unit amplitude components having random-phase angles $\phi_i(\omega)$. If $\phi_i(\omega)$ and $\phi_j(\omega)$ are uniformly distributed random-phase angles, the relations

$$E[\eta_{\phi_i}(i\omega)\eta^*_{\phi_j}(i\omega)] = 0 \quad \text{if } i \neq j$$

$$E[\eta_{\phi_i}(i\omega)\eta^*_{\phi_j}(i\omega)] = 1 \quad \text{if } i = j \tag{42.10}$$

will be satisfied, where the symbol $E[\ ]$ represents ensemble average. It can easily be shown that the ensemble of motions generated using Eq. (42.9) will satisfy Eq. (42.7). Thus, if the rock-outcrop motions at all pier support locations are generated from the corresponding motions at the control point location using Eq. (42.9), the resulting motions at all locations will satisfy, on an ensemble basis, the coherency functions specified for the site. Since the matrix $\boldsymbol{L}(i\omega)$ in Eq. (42.9) is a lower triangular matrix having its diagonal elements equal to unity, the generation of coherency compatible motions at all pier locations can be achieved by marching from one pier location to the next in a sequential manner starting with the control pier location.

In generating the coherency compatible motions using Eq. (42.9), the phase angle shifts at various pier locations due to the single plane-wave passage at the constant speed V_{bridge} defined by Eq. (42.3) can be incorporated into the term $\boldsymbol{\eta}_{\phi_i}(i\omega)$. Since the motions at the control point location are response spectrum compatible, the coherency compatible motions generated at all other pier locations using the above-described procedure will be approximately response spectrum compatible. However, an improvement on their response spectrum compatibility is generally required, which can be done by adjusting their Fourier amplitudes but keeping their Fourier phase angles unchanged. By keeping these angles unchanged, the coherencies among the adjusted motions are not affected. Consequently, the adjusted motions will not only be response spectrum compatible, but will also be coherency compatible.

In generating the response spectrum- and coherency-compatible motions at all pier locations by the procedure described above, the ground motion attenuation effect has been ignored. For a long bridge located close to the controlling seismic source, attenuation of motion with distance away from the control pier location should be considered. This can be achieved by scaling the generated motions at various pier locations by appropriate scaling factors determined from an appropriate ground motion attenuation relation. The acceleration time histories generated for all pier locations should be integrated to obtain their corresponding velocity and displacement time histories, which should be checked to ensure against having numerically generated baseline drifts. Relative displacement time histories between the control pier location and successive pier locations should also be checked to ensure that they are reasonable. The rock-outcrop motions finally obtained should then be used in appropriate site-response analyses to develop the corresponding free-field soil motions required in conducting the SFSI analyses for each pier location.

42.4.3 Free-Field Soil Motions

As previously mentioned, the seismic inputs to large bridges are defined in terms of the expected free-field soil motions at discrete elevations over the entire depth of each foundation. Such motions must be evaluated through location-specific site-response analyses using the corresponding previously described rock-outcrop free-field motions as inputs to appropriately defined soil–bedrock

models. Usually, as mentioned previously, these models are based on the assumption that the horizontal and vertical free-field soil motions are produced by upward/downward propagation of one-dimensional shear and compression waves, respectively, as caused by the upward propagation of incident waves in the underlying rock or firm soil formation. Consistent with these types of motion, it is assumed that the local soil medium surrounding each foundation consists of uniform horizontal layers of infinite lateral extent. Wave reflections and refractions will occur at all interfaces of adjacent layers, including the soil–bedrock interface, and reflections of the waves will occur at the soil surface. Computer program SHAKE [4,44] is most commonly used to carry out the above-described one-dimensional type of site-response analysis. For a long bridge having a widely varying soil profile from end to end, such site-response analyses must be repeated for different soil columns representative of the changing profile.

The cyclic free-field soil deformations produced at a particular bridge site by a maximum expected earthquake are usually of the nonlinear hysteretic form. Since the SHAKE computer program treats a linear system, the soil column being analyzed must be modeled in an equivalent linearized manner. To obtain the equivalent linearized form, the soil parameters in the model are modified after each consecutive linear time history response analysis is complete, which continues until convergence to strain-compatible parameters are reached.

For generating horizontal free-field motions produced by vertically propagating shear waves, the needed equivalent linear soil parameters are the shear modulus G and the hysteretic damping ratio β. These parameters, as prepared by Vucetic and Dobry [36] in 1991 for clay and by Sun et al. [37] in 1988 and by the Electric Power Research Institute (EPRI) for sand, are plotted in Figures 42.6 and 42.7, respectively, as functions of shear strain γ. The shear modulus is plotted in its nondimensional form G/G_{max} where G_{max} is the *in situ* shear modulus at very low strains ($\gamma \leq 10^{-4}\%$). The shear modulus G must be obtained from cyclic shear tests, while G_{max} can be obtained using $G_{max} = \rho V_s^2$ in which ρ is mass density of the soil and V_s is the *in situ* shear wave velocity obtained by field measurement. If shear wave velocities are not available, G_{max} can be estimated using published empirical formulas which correlate shear wave velocity or shear modulus with blow counts and/or other soil parameters [38–43]. To obtain the equivalent linearized values of G/G_{max} and β following each consecutive time history response analysis, values are taken from the G/G_{max} vs. γ and β vs. γ relations at the effective shear strain level defined as $\gamma_{eff} = \alpha\gamma_{max}$ in which γ_{max} is the maximum shear strain reached in the last analysis and α is the effective strain factor. In the past, α has usually been assigned the value 0.65; however, other values have been proposed (e.g., Idriss and Sun [44]). The equivalent linear time history response analyses are performed in an iterative manner, with soil parameter adjustments being made after each analysis, until the effective shear strain converges to essentially the same value used in the previous iteration [45]. This normally takes four to eight iterations to reach 90 to 95% of full convergence when the effective shear strains do not exceed 1 to 2%. When the maximum strain exceeds 2%, a nonlinear site-response analysis is more appropriate. Computer programs available for this purpose are DESRA [46], DYNAFLOW [47], DYNAID [48], and SUMDES [49].

For generating vertical free-field motions produced by vertically propagating compression waves, the needed soil parameters are the low-strain constrained elastic modulus $E_p = \rho V_p^2$, where V_p is the compression wave velocity, and the corresponding damping ratio. The variations of these soil parameters with compressive strain have not as yet been well established. At the present time, vertical site-response analyses have generally been carried out using the low-strain constrained elastic moduli, E_p, directly and the strain-compatible damping ratios obtained from the horizontal response analyses, but limited to a maximum value of 10%, without any further strain-compatibility iterations. For soils submerged in water, the value of E_p should not be less than the compression wave velocity of water.

Having generated acceleration free-field time histories of motion using the SHAKE computer program, the corresponding velocity and displacement time histories should be obtained through

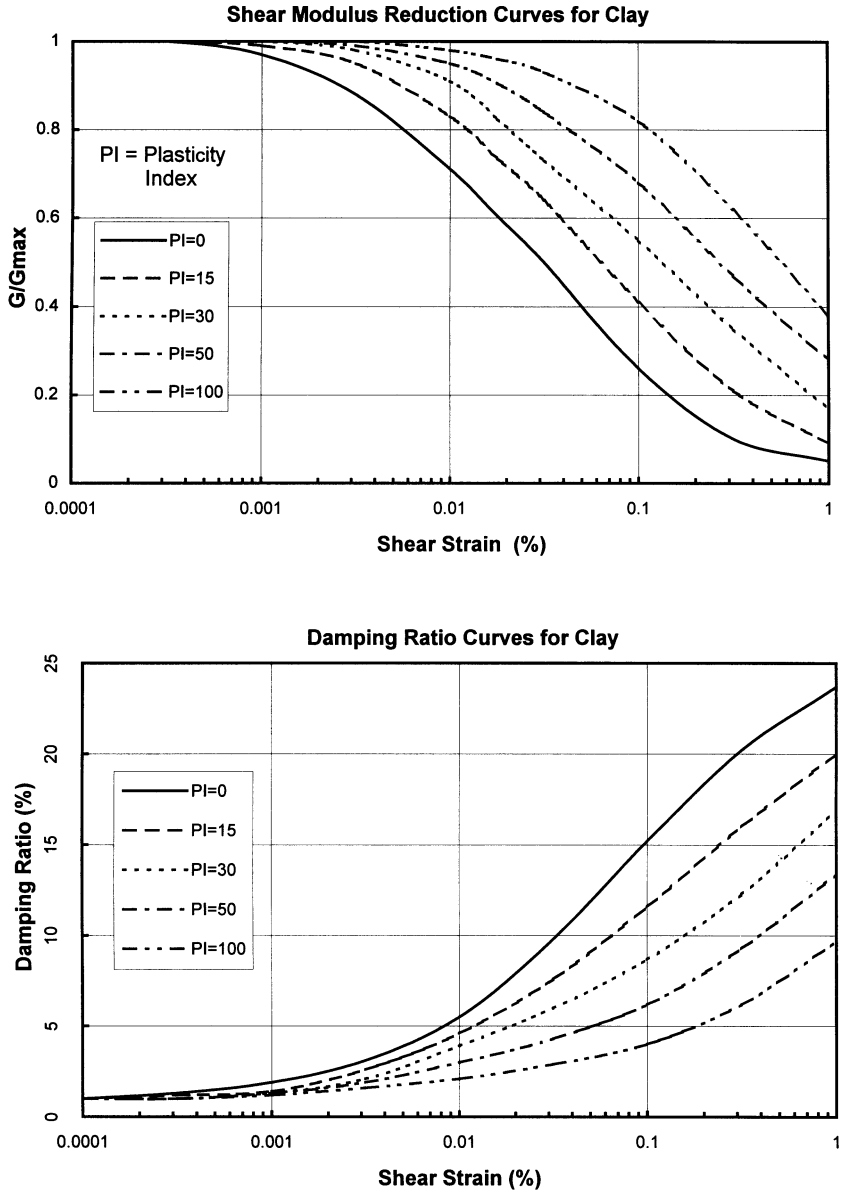

FIGURE 42.6 Equivalent linear shear modulus and hysteretic damping ratio as functions of shear strain for clay. (Source: Vucetic, M. and Dobry, R., *J. Geotech. Eng. ASCE*, 117(1), 89-107, 1991. With permission.)

single and double integrations of the acceleration time histories. Should unrealistic drifts appear in the displacement time histories, appropriate corrections should be applied. Should such drifts appear in a straight-line fashion, it usually indicates that the durations specified for Fourier transforming the recorded accelerograms are too short; thus, increasing these durations will usually correct the problem. If the baseline drifts depart significantly from a simple straight line, this tends to indicate that the analysis results may be unreliable; in which case, they should be carefully checked before being used. Time histories of free-field relative displacement between pairs of pier locations should also be generated and then be checked to judge the reasonableness of the results obtained.

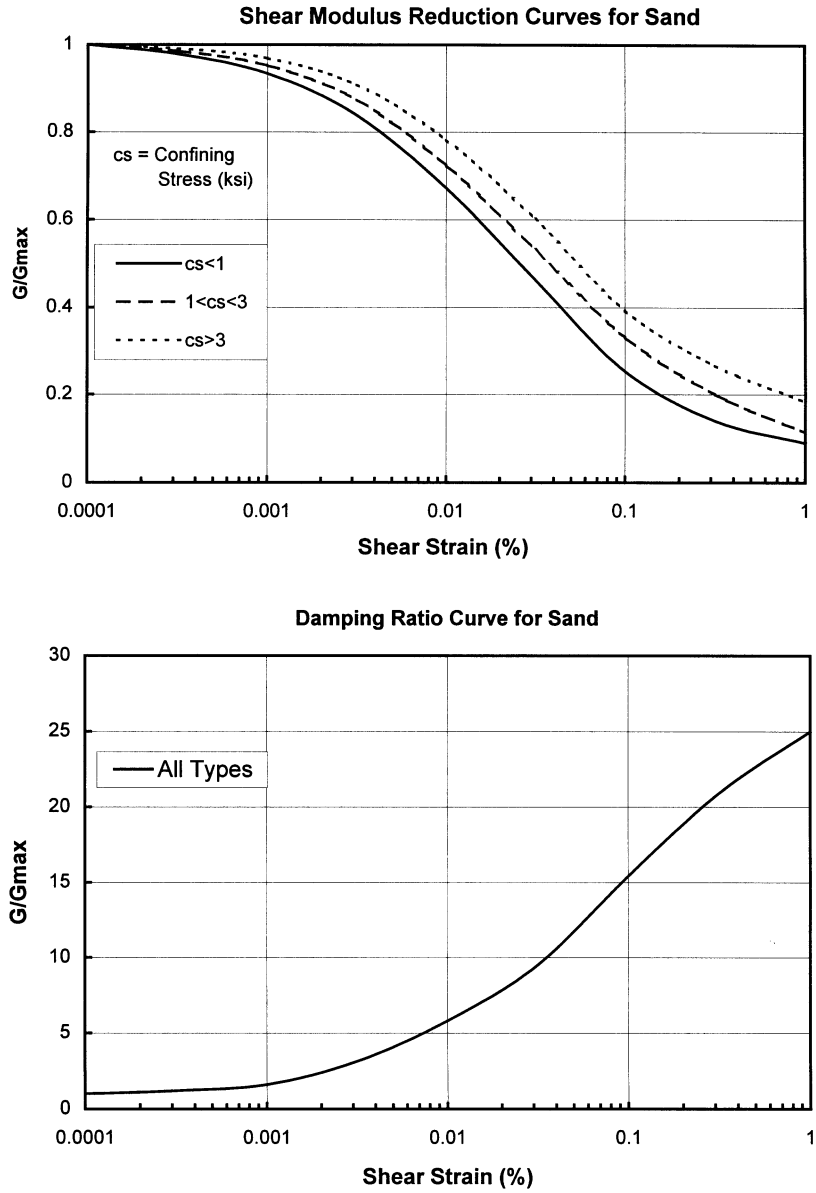

FIGURE 42.7 Equivalent linear shear modulus and hysteretic damping ratio as functions of shear strain for sand. (Source: Sun, J. I. et al., Reort No. UBC/EERC-88/15, Earthquake Engineer Research Center, University of California, Berkeley, 1988.)

42.5 Characterization of Soil–Foundation System

The core of the dynamic SFSI problem for a bridge is the interaction between its structure–foundation system and the supporting soil medium, which, for analysis purposes, can be considered to be a full half-space. The fundamental step in solving this problem is to characterize the constitutive relations between the dynamic forces acting on each foundation of the bridge at its interface boundary with the soil and the corresponding foundation motions, expressed in terms of the displacements, velocities, and accelerations. Such forces are here called the soil–foundation interaction forces. For a bridge subjected to externally applied loadings, such as dead, live, wind, and

wave loadings, these SFI forces are functions of the foundation motions only; however, for a bridge subjected to seismic loadings, they are functions of the free-field soil motions as well.

Let h be the total number of degrees of freedom (DOF) of the bridge foundations as defined at their soil–foundation interface boundaries; $\boldsymbol{u}_h(t)$, $\dot{\boldsymbol{u}}_h(t)$, and $\ddot{\boldsymbol{u}}_h(t)$ be the corresponding foundation displacement, velocity, and acceleration vectors, respectively; and $\bar{\boldsymbol{u}}_h(t)$, $\dot{\bar{\boldsymbol{u}}}_h(t)$, and $\ddot{\bar{\boldsymbol{u}}}_h(t)$ be the free-field soil displacement, velocity, and acceleration vectors in the h DOF, respectively; and let $\boldsymbol{f}_h(t)$ be the corresponding SFI force vector. By using these notations, characterization of the SFI forces under seismic conditions can be expressed in the general vectorial functional form:

$$\boldsymbol{f}_h(t) = \Im_h\ (\boldsymbol{u}_h(t),\ \dot{\boldsymbol{u}}_h(t),\ \ddot{\boldsymbol{u}}_h(t),\ \bar{\boldsymbol{u}}_h(t)\ \ \dot{\bar{\boldsymbol{u}}}_h(t),\ \ddot{\bar{\boldsymbol{u}}}_h(t)) \tag{42.11}$$

Since the soils in the local region immediately surrounding each foundation may behave nonlinearly under imposed foundation loadings, the form of $\Im_h$ is, in general, a nonlinear function of displacements $\boldsymbol{u}_h(t)$ and $\bar{\boldsymbol{u}}_h(t)$ and their corresponding velocities and accelerations.

For a capacity evaluation, the nonlinear form of $\Im_h$ should be retained and used directly for determining the SFI forces as functions of the foundation and soil displacements. Evaluation of this form should be based on a suitable nonlinear model for the soil medium coupled with appropriate boundary conditions, subjected to imposed loadings which are usually much simplified compared with the actual induced loadings. This part of the evaluation will be discussed further in Section 42.8.

For a demand evaluation, the nonlinear form of $\Im_h$ is often linearized and then transformed to the frequency domain. Letting $\boldsymbol{u}_h(i\omega)$, $\dot{\boldsymbol{u}}_h(i\omega)$, $\ddot{\boldsymbol{u}}_h(i\omega)$, $\bar{\boldsymbol{u}}_h(i\omega)$, $\dot{\bar{\boldsymbol{u}}}_h(i\omega)$, $\ddot{\bar{\boldsymbol{u}}}_h(i\omega)$, and $\boldsymbol{f}_h(i\omega)$ be the Fourier transforms of $\boldsymbol{u}_h(t)$, $\dot{\boldsymbol{u}}_h(t)$, $\ddot{\boldsymbol{u}}_h(t)$, $\bar{\boldsymbol{u}}_h(t)$, $\dot{\bar{\boldsymbol{u}}}_h(t)$, $\ddot{\bar{\boldsymbol{u}}}_h(t)$, and $\boldsymbol{f}_h(t)$, respectively, and making use of the relations

$$\dot{\boldsymbol{u}}_h(i\omega) = i\omega\,\boldsymbol{u}_h(i\omega);\qquad \ddot{\boldsymbol{u}}_h(i\omega) = -\omega^2\,\boldsymbol{u}_h(i\omega)$$

and

$$\dot{\bar{\boldsymbol{u}}}_h(i\omega) = i\omega\,\bar{\boldsymbol{u}}_h(i\omega);\qquad \ddot{\bar{\boldsymbol{u}}}_h(i\omega) = -\omega^2\,\bar{\boldsymbol{u}}_h(i\omega), \tag{42.12}$$

Equation (42.11) can be cast into the more convenient form:

$$\boldsymbol{f}_h(i\omega) = \Im_h\ (\ u_h(i\omega), \bar{\boldsymbol{u}}_h(i\omega)) \tag{42.13}$$

To characterize the linear functional form of $\Im_h$, it is necessary to solve the dynamic boundary-value problem for a half-space soil medium subjected to force boundary conditions prescribed at the soil–foundation interfaces. This problem is referred to here as the "soil impedance" problem, which is a part of the foundation impedance problem referred to earlier in Section 42.2.2.

In linearized form, Eq. (42.13) can be expressed as

$$\boldsymbol{f}_h(i\omega) = \boldsymbol{G}_{hh}(i\omega)\ \ \{\boldsymbol{u}_h(i\omega) - \bar{u}_h(i\omega)\} \tag{42.14}$$

in which $\boldsymbol{f}_h(i\omega)$ represents the force vector acting on the soil medium by the foundation and the matrix $\boldsymbol{G}_{hh}(i\omega)$ is a complex, frequency-dependent coefficient matrix called here the "soil impedance matrix."

Define a force vector $\bar{\boldsymbol{f}}_h(i\omega)$ by the relation

$$\bar{\boldsymbol{f}}_h(i\omega) = \boldsymbol{G}_{hh}(i\omega)\ \ \bar{\boldsymbol{u}}_h(i\omega) \tag{42.15}$$

This force vector represents the internal dynamic forces acting on the bridge foundations at their soil–foundation interface boundaries resulting from the free-field soil motions when the foundations are held fixed, i.e., $\boldsymbol{u}_h(i\omega) = \mathbf{0}$. The force vector $\bar{\boldsymbol{f}}_h(i\omega)$ as defined in Eq. (42.15) is the "seismic driving force" vector mentioned previously in Section 42.2.2. Depending upon the type of bridge foundation, the characterization of the soil impedance matrix $\boldsymbol{G}_{hh}(i\omega)$ and associated free-field soil input motion vector $\bar{\boldsymbol{u}}_h(i\omega)$ for demand analysis purposes may be established utilizing different soil models as described below.

42.5.1 Elastodynamic Model

As mentioned in Section 42.3.1, for a large bridge foundation such as a large spread footing, caisson, or single or multiple shafts having very large diameters, for which the nonlinearities occurring in the local soil region immediately adjacent to the foundation are small, the soil impedance matrix $\boldsymbol{G}_{hh}(i\omega)$ can be evaluated utilizing the dynamic Green's functions (dynamic displacements of the soil medium due to harmonic point-load excitations) obtained from the solution of a dynamic boundary-value problem of a linear damped-elastic half-space soil medium subjected to harmonic point loads applied at each of the h DOF on the soil–foundation interface boundaries. Such solutions have been obtained in analytical form for a linear damped-elastic continuum half-space soil medium by Apsel [50] in 1979. Because of complexities in the analytical solution, dynamic Green's functions have only been obtained for foundations having relatively simple soil–foundation interface geometries, e.g., rectangular, cylindrical, or spherical soil–foundation interface geometries, supported in simple soil media. In practical applications, the dynamic Green's functions are often obtained in numerical forms based on a finite-element discretization of the half-space soil medium and a corresponding discretization of the soil–foundation interface boundaries using a computer program such as SASSI [51], which has the capability of properly simulating the wave radiation boundary conditions at the far field of the half-space soil medium. The use of finite-element soil models to evaluate the dynamic Green's functions in numerical form has the advantage that foundations having arbitrary soil–foundation interface geometries can be easily handled; it, however, suffers from the disadvantage that the highest frequency, i.e., cutoff frequency, of motion for which a reliable solution can be obtained is limited by size of the finite element used for modeling the soil medium.

Having evaluated the dynamic Green's functions using the procedure described above, the desired soil impedance matrix can then be obtained by inverting, frequency-by-frequency, the "soil compliance matrix," which is the matrix of Green's function values evaluated for each specified frequency ω. Because the dynamic Green's functions are complex valued and frequency dependent, the coefficients of the resulting soil impedance matrix are also complex-valued and frequency dependent. The real parts of the soil impedance coefficients represent the dynamic stiffnesses of the soil medium which also incorporate the soil inertia effects; the imaginary parts of the coefficients represent the energy losses resulting from both soil material damping and radiation of stress waves into the far-field soil medium. Thus, the soil impedance matrix as developed reflects the overall dynamic characteristics of the soil medium as related to the motion of the foundation at the soil–foundation interfaces.

Because of the presence of the foundation excavation cavities in the soil medium, the vector of free-field soil motions $\bar{\boldsymbol{u}}_h(i\omega)$ prescribed at the soil–foundation interface boundaries has to be derived from the seismic input motions of the free-field soil medium without the foundation excavation cavities as described in Section 42.4. The derivation of the motion vector $\bar{\boldsymbol{u}}_h(i\omega)$ requires the solution of a dynamic boundary-value problem for the free-field half-space soil medium having foundation excavation cavities subjected to a specified seismic wave input such that the resulting solution satisfies the traction-free conditions at the surfaces of the foundation excavation cavities. Thus, the resulting seismic response motions, $\bar{\boldsymbol{u}}_h(i\omega)$, reflect the effects of seismic wave scattering due to the presence of the cavities. These motions are, therefore, referred to here as the "scattered free-field soil input motions."

The effects of seismic wave scattering depend on the relative relation between the characteristic dimension, l_f, of the foundation and the specific seismic input wave length, λ, of interest, where

$\lambda = 2\pi V_s/\omega$ or $2\pi V_p/\omega$ for vertically propagating plane shear or compression waves, respectively; V_s and V_p are, as defined previously, the shear and compression wave velocities of the soil medium, respectively. If the input seismic wave length λ is much longer than the characteristic length l_f, the effect of wave scattering will be negligible; on the other hand, when $\lambda \leq l_f$, the effect of wave scattering will be significant. Since the wave length λ is a function of the frequency of input motion, the effect of wave scattering is also frequency dependent. Thus, it is evident that the effect of wave scattering is much more important for a large bridge foundation, such as a large caisson or a group of very large diameter shafts, than for a small foundation having a small characteristic dimension, such as a slender-pile group; it can also be readily deduced that the scattering effect is more significant for foundations supported in soft soil sites than for those in stiff soil sites.

The characterization of the soil impedance matrix utilizing an elastodynamic model of the soil medium as described above requires soil material characterization constants which include (1) mass density, ρ; (2) shear and constrained elastic moduli, G and E_p (or shear and compression wave velocities, V_s and V_p); and (3) constant-hysteresis damping ratio, β. As discussed previously in Section 42.4.3, the soil shear modulus decreases while the soil hysteresis damping ratio increases as functions of soil shear strains induced in the free-field soil medium due to the seismic input motions. The effects of these so-called global soil nonlinearities can be easily incorporated into the soil impedance matrix based on an elastodynamic model by using the free-field-motion-induced strain-compatible soil shear moduli and damping ratios as the soil material constants in the evaluation of the dynamic Green's functions. For convenience of later discussions, the soil impedance matrix, $\boldsymbol{G}_{hh}(i\omega)$, characterized using an elastodynamic model will be denoted by the symbol $\boldsymbol{G}^e_{hh}(i\omega)$.

42.5.2 Empirical *p–y* Model

As discussed in Section 42.3.2, for a slender-pile group foundation for which soil nonlinearities occurring in the local soil regions immediately adjacent to the piles dominate the behavior of the foundation under loadings, the characterization of the soil resistances to pile deflections has often relied on empirically derived *p–y* curves for lateral resistance and *t–z* and *Q–d* curves for axial resistance. For such a foundation, the characterization of the soil impedance matrix needed for demand analysis purposes can be made by using the secant moduli derived from the nonlinear *p–y, t–z,* and *Q–d* curves, as indicated schematically in Figure 42.2. Since the development of these empirical curves has been based upon static or pseudo-static test results, it does not incorporate the soil inertia and material damping effects. Thus, the resulting soil impedance matrix developed from the secant moduli of the *p–y, t–z,* and *Q–d* curves reflects only the static soil stiffnesses but not the soil inertia and soil material damping characteristics. Hence, the soil impedance matrix so obtained is a real-valued constant coefficient matrix applicable at the zero frequency ($\omega = 0$); it, however, is a function of the foundation displacement amplitude. This matrix is designated here as $\boldsymbol{G}^s_{hh}(0)$ to differentiate it from the soil impedance matrix $\boldsymbol{G}^e_{hh}(i\omega)$ defined previously. Thus, Eq. (42.14) in this case is given by

$$\boldsymbol{f}_h(i\omega) = \boldsymbol{G}^s_{hh}(0)\{\boldsymbol{u}_h(i\omega) - \bar{\boldsymbol{u}}_h(i\omega)\} \tag{42.16}$$

where $\boldsymbol{G}^s_{hh}(0)$ depends on the amplitudes of the relative displacement vector $\Delta\boldsymbol{u}_h(i\omega)$ defined by

$$\Delta\boldsymbol{u}_h(i\omega) = \boldsymbol{u}_h(i\omega) - \bar{\boldsymbol{u}}_h(i\omega) \tag{42.17}$$

As mentioned previously in Section 42.3.2, the construction of the *p–y, t–z,* and *Q–d* curves depends only on the strength parameters but not on the stiffness parameters of the soil medium; thus, the effects of global soil nonlinearities on the dynamic stiffnesses of the soil medium, as caused by soil shear modulus decrease and soil-damping increase as functions of free-field-motion-induced soil

shear strains, cannot be incorporated into the soil impedance matrix developed from these curves. Furthermore, since these curves are developed on the basis of results from field tests in which there are no free-field ground-motion-induced soil deformations, the effects of such global soil nonlinearities on the soil strength characterization parameters and hence the *p–y, t–z,* and *Q–d* curves cannot be incorporated.

Because of the small cross-sectional dimensions of slender piles, the seismic wave-scattering effect due to the presence of pile cavities is usually negligible; thus, the scattered free-field soil input motions $\bar{\boldsymbol{u}}_h(i\omega)$ in this case are often taken to be the same as the free-field soil motions when the cavities are not present.

42.5.3 Hybrid Model

From the discussions in the above two sections, it is clear that characterization of the SFI forces for demand analysis purposes can be achieved using either an elastodynamic model or an empirical *p–y* model for the soil medium, each of which has its own merits and deficiencies. The elastodynamic model is capable of incorporating soil inertia, damping (material and radiation), and stiffness characteristics, and it can incorporate the effects of global soil nonlinearities induced by the free-field soil motions in an equivalent linearized manner. However, it suffers from the deficiency that it does not allow for easy incorporation of the effects of local soil nonlinearities. On the contrary, the empirical *p–y* model can properly capture the effects of local soil nonlinearities in an equivalent linearized form; however, it suffers from the deficiencies of not being able to simulate soil inertia and damping effects properly, and it cannot treat the effects of global soil nonlinearities. Since the capabilities of the two models are mutually complementary, it is logical to combine the elastodynamic model with the empirical *p–y* model in a series form such that the combined model has the desired capabilities of both models. This combined model is referred to here as the "hybrid model."

To develop the hybrid model, let the relative displacement vector, $\Delta\boldsymbol{u}_h(i\omega)$, between the foundation displacement vector $\boldsymbol{u}_h(i\omega)$ and the scattered free-field soil input displacement vector $\bar{\boldsymbol{u}}_h(i\omega)$, as defined by Eq. (42.17), be decomposed into a component representing the relative displacements at the soil–foundation interface boundary resulting from the elastic deformation of the global soil medium outside of the soil–foundation interface, designated as $\Delta\boldsymbol{u}_h^e(i\omega)$, and a component representing the relative displacements at the same boundary resulting from the inelastic deformations of the local soil regions adjacent the foundation, designated as $\Delta\boldsymbol{u}_h^i(i\omega)$; thus,

$$\Delta\boldsymbol{u}_h(i\omega) = \Delta\boldsymbol{u}_h^i(i\omega) + \Delta\boldsymbol{u}_h^e(i\omega) \tag{42.18}$$

Let $\boldsymbol{f}_h^e(i\omega)$ represent the elastic force vector which can be characterized in terms of the elastic relative displacement vector $\boldsymbol{u}_h^e(i\omega)$ using the elastodynamic model, in which case

$$\boldsymbol{f}_h^e(i\omega) = \boldsymbol{G}_{hh}^e(i\omega)\Delta\boldsymbol{u}_h^e(i\omega) \tag{42.19}$$

where $\boldsymbol{G}_{hh}^e(i\omega)$ is the soil impedance matrix as defined previously in Section 42.5.1, which can be evaluated using an elastodynamic model. Let $\boldsymbol{f}_h^i(i\omega)$ represent the inelastic force vector which is assumed to be related to $\Delta\boldsymbol{u}_h^i(i\omega)$ by the relation

$$\boldsymbol{f}_h^i(i\omega) = \boldsymbol{G}_{hh}^i(i\omega)\Delta\boldsymbol{u}_h^i(i\omega) \tag{42.20}$$

The characterization of the matrix $\boldsymbol{G}_{hh}^i(i\omega)$ can be accomplished by utilizing the soil secant stiffness matrix $\boldsymbol{G}_{hh}^s(0)$ developed from the empirical *p–y* model by the procedure discussed below.

Solving Eqs. (42.19) and (42.20) for $\Delta\boldsymbol{u}_h^e(i\omega)$ and $\Delta\boldsymbol{u}_h^i(i\omega)$, respectively, substituting these relative displacement vectors into Eq. (42.18), and making use of the force continuity condition

that $\boldsymbol{f}_h^e(i\omega) = \boldsymbol{f}_h^i(i\omega)$, since the elastodynamic model and the inelastic local model are in series, one obtains

$$\boldsymbol{f}_h(i\omega) = \left\{[\boldsymbol{G}_{hh}^i(i\omega)]^{-1} + [\boldsymbol{G}_{hh}^e(i\omega)]^{-1}\right\}^{-1} \Delta\boldsymbol{u}_h(i\omega) \tag{42.21}$$

Comparing Eq. (42.14) with Eq. (42.21), one finds that by using the hybrid model, the soil impedance matrix is given by

$$\boldsymbol{G}_{hh}(i\omega) = \left\{[\boldsymbol{G}_{hh}^i(i\omega)]^{-1} + [\boldsymbol{G}_{hh}^e(i\omega)]^{-1}\right\}^{-1} \tag{42.22}$$

Since the soil impedance matrix $\boldsymbol{G}_{hh}^s(i\omega)$ is formed by the static secant moduli of the nonlinear *p–y, t–z,* and *Q–d* curves when $\omega = 0$, Eq. (42.22) becomes

$$\boldsymbol{G}_{hh}^s(0) = \left\{[\boldsymbol{G}_{hh}^i(0)]^{-1} + [\boldsymbol{G}_{hh}^e(0)]^{-1}\right\}^{-1} \tag{42.23}$$

where $\boldsymbol{G}_{hh}^s(0)$ is the soil stiffness matrix derived from the secant moduli of the nonlinear *p–y, t–z,* and *Q–d* curves. Solving Eq. (42.23), for $\boldsymbol{G}_{hh}^i(0)$ gives

$$\boldsymbol{G}_{hh}{}^i(0) = \left\{[\boldsymbol{G}_{hh}^s(0)]^{-1} - [\boldsymbol{G}_{hh}^e(0)]^{-1}\right\}^{-1} \tag{42.24}$$

Thus, Eq. (42.22) can be expressed in the form

$$\boldsymbol{G}_{hh}(i\omega) = \left\{[\boldsymbol{G}_{hh}^i(0)]^{-1} + [\boldsymbol{G}_{hh}^e(i\omega)]^{-1}\right\}^{-1} \tag{42.25}$$

From Eq. (42.25), it is evident that when $\Delta\boldsymbol{u}_h{}^i(i\omega) << \Delta\boldsymbol{u}_h{}^e(i\omega)$, $\boldsymbol{G}_{hh}(i\omega) \rightarrow \boldsymbol{G}_{hh}^e(i\omega)$; however, when $\Delta\boldsymbol{u}_h{}^i(i\omega) >> \Delta\boldsymbol{u}_h{}^e(i\omega)$, $\boldsymbol{G}_{hh}(i\omega) \rightarrow \boldsymbol{G}_{hh}^i(0) \rightarrow \boldsymbol{G}_{hh}^s(0)$. Thus, the hybrid model represented by this equation converges to the elastodynamic model when the local inelastic soil deformations are relatively small, as for the case of a large footing, caisson, or very large diameter shaft foundation, whereas it converges to the empirical *p–y* model when the local inelastic soil deformations are relatively much larger, as for the case of a slender-pile group foundation. For a moderately large diameter shaft foundation, the local inelastic and global elastic soil deformations may approach a comparable magnitude; in which case, the use of a hybrid model to develop the soil impedance matrix as described above can properly represent both the global elastodynamic and local inelastic soil behaviors.

As local soil nonlinearities are induced by the relative displacements between the foundation and the scattered free-field soil input motions, they do not affect the scattering of free-field soil motions due to the traction-free conditions present at the surface of the foundation cavities. Therefore, in applying the hybrid model described above, the scattered free-field soil input motion vector $\bar{\boldsymbol{u}}_h(i\omega)$ should still be derived using the elastodynamic model described in Section 42.5.1.

42.6 Demand Analysis Procedures

42.6.1 Equations of Motion

The seismic response of a complete bridge system involves interactions between the structure and its supporting foundations and between the foundations and their surrounding soil media. To develop the equations of motion governing the response of this system in discrete (finite-element)

form, let s denote the number of DOF in the structure, excluding its f DOF at the structure/foundation interface locations, and let g denote the number of DOF in the foundations, also excluding the f DOF but including the h DOF at all soil–foundation interfaces as defined in Section 42.5. Corresponding with those DOF, let vectors $\boldsymbol{u}_s(t)$, $\boldsymbol{u}_f(t)$, and $\boldsymbol{u}_g(t)$ contain the total displacement time histories of motion at the DOF s, f, and g, respectively.

Linear Modeling

Since the soil medium surrounding all foundations is continuous and of infinite extent, a rigorous model of a complete bridge system must contain stiffness and damping coefficients which are dependent upon the excitation (or response) frequencies. Such being the case, the corresponding equations of motion of the complete system having n DOF ($n = s + f + g$) must rigorously be represented in the frequency domain.

Considering the coupled structure–foundation system as a free-free (no boundary constraints) system having externally applied forces $-\boldsymbol{f}_h(t)$ acting in the h DOF, its equations of motion can be expressed in the frequency-domain form:

$$\begin{bmatrix} \boldsymbol{D}_{ss}(i\omega) & \boldsymbol{D}_{sf}(i\omega) & \boldsymbol{0} \\ \boldsymbol{D}_{sf}^T(i\omega) & \boldsymbol{D}_{ff}(i\omega) & \boldsymbol{D}_{fg}(i\omega) \\ \boldsymbol{0} & \boldsymbol{D}_{sf}^T(i\omega) & \boldsymbol{D}_{gg}(i\omega) \end{bmatrix} \begin{Bmatrix} \boldsymbol{u}_s(i\omega) \\ \boldsymbol{u}_f(i\omega) \\ \boldsymbol{u}_g(i\omega) \end{Bmatrix} = \begin{Bmatrix} \boldsymbol{0} \\ \boldsymbol{0} \\ \boldsymbol{f}_g(i\omega) \end{Bmatrix} \tag{42.26}$$

in which $\boldsymbol{u}_s(i\omega)$, $\boldsymbol{u}_f(i\omega)$, $\boldsymbol{u}_g(i\omega)$, and $\boldsymbol{f}_g(i\omega)$ are the Fourier transforms of vectors $\boldsymbol{u}_s(t)$, $\boldsymbol{u}_f(t)$, $\boldsymbol{u}_g(t)$, and $\boldsymbol{f}_g(t)$, respectively; and matrices $\boldsymbol{D}_{ij}(i\omega)$, $i, j = s, f, g$, are the corresponding impedance (dynamic stiffness) matrices. The g components in vectors $\boldsymbol{u}_g(i\omega)$ and $\boldsymbol{f}_g(i\omega)$ are ordered such that their last h components make up vectors $\boldsymbol{u}_h(i\omega)$ and $-\boldsymbol{f}_h(i\omega)$, respectively, with all other components being equal to zero.

For a viscously damped linear structure–foundation system, the impedance matrices $\boldsymbol{D}_{ij}(i\omega)$ are of the form:

$$\boldsymbol{D}_{ij}(i\omega) = \boldsymbol{K}_{ij} + i\omega\boldsymbol{C}_{ij} - \omega^2\boldsymbol{M}_{ij} \qquad i, j = s, f, g \tag{42.27}$$

in which $\boldsymbol{K}_{ij}$, $\boldsymbol{C}_{ij}$, and $\boldsymbol{M}_{ij}$ are the standard stiffness, damping, and mass matrices, respectively, which would appear in the equations of motion of the system if expressed in the time domain. For a constant-hysteresis-damped linear system, the impedance matrices are given by

$$\boldsymbol{D}_{ij}(i\omega) = \boldsymbol{K}_{ij}^* - \omega^2\boldsymbol{M}_{ij} \qquad i, j = s, f, g \tag{42.28}$$

in which $\boldsymbol{K}_{ij}^*$ is a complex stiffness matrix obtained by assembling individual finite-element matrices $\boldsymbol{K}^{*(m)}$ of the form

$$\boldsymbol{K}^{*(m)} \equiv \left\{1 - 2(\beta^{(m)})^2 + 2i\beta^{(m)}\sqrt{1-(\beta^{(m)})^2}\right\}\boldsymbol{K}^{(m)} \doteq (1 + 2i\beta^{(m)})\boldsymbol{K}^{(m)} \tag{42.29}$$

where $\boldsymbol{K}^{(m)}$ denotes the standard elastic stiffness matrix for finite element m as used in the assembly process to obtain matrix $\boldsymbol{K}_{ij}$ and $\beta^{(m)}$ is a damping ratio specified appropriately for the material used in finite-element m [56].

The hysteretic form of damping represented in Eq. (42.28) is the more appropriate form to use for two reasons: (1) it is easy to accommodate different damping ratios for the different materials used in the system and (2) the resulting modal damping is independent of excitation (or response)

frequency ω, consistent with test evidence showing that real damping is indeed essentially independent of this frequency. As noted by the form of Eq. (42.27), viscous damping is dependent upon frequency ω, contrary to test results; thus, preference should definitely be given to the use of hysteretic damping for linear systems which can be solved in the frequency domain. Hysteretic damping is unfortunately incompatible with solutions in the time domain.

Vector $-\boldsymbol{f}_h(i\omega)$, which makes up the last h components in force vector $\boldsymbol{f}_g(i\omega)$ appearing in Eq. (42.26), represents, as defined in Section 42.5, the internal SFI forces at the soil–foundation interfaces when the entire coupled soil–foundation–structure system is responding to the free-field soil input motions. Therefore, to solve the SFSI problem, this vector must be characterized in terms of the foundation displacement vector $\boldsymbol{u}_h(i\omega)$ and the scattered free-field soil displacement vector $\bar{\boldsymbol{u}}_h(i\omega)$. As discussed previously in Section 42.5, for demand analysis purposes, this vector can be linearized to the form

$$-\boldsymbol{f}_h(i\omega) = \boldsymbol{G}_{hh}(i\omega)\left\{\bar{\boldsymbol{u}}_h(i\omega) - \boldsymbol{u}_h(i\omega)\right\} \tag{42.30}$$

in which $-\boldsymbol{f}_h(i\omega)$ represents the force vector acting on the foundations from the soil medium and $\boldsymbol{G}_{hh}(i\omega)$ is the soil impedance matrix which is complex valued and frequency dependent.

Substituting Eq. (42.30) into Eq. (42.26), the equations of motion of the complete bridge system become

$$\begin{bmatrix} \boldsymbol{D}_{ss}(i\omega) & \boldsymbol{D}_{sf}(i\omega) & \boldsymbol{0} \\ \boldsymbol{D}_{sf}^T(i\omega) & \boldsymbol{D}_{ff}(i\omega) & \boldsymbol{D}_{fg}(i\omega) \\ \boldsymbol{0} & \boldsymbol{D}_{fg}^T(i\omega) & [\boldsymbol{D}_{gg}(i\omega) + G_{gg}(i\omega)] \end{bmatrix} \begin{Bmatrix} \boldsymbol{u}_s(i\omega) \\ \boldsymbol{u}_f(i\omega) \\ \boldsymbol{u}_g(i\omega) \end{Bmatrix} = \begin{Bmatrix} \boldsymbol{0} \\ \boldsymbol{0} \\ \bar{\boldsymbol{f}}_g(i\omega) \end{Bmatrix} \tag{42.31}$$

in which

$$\boldsymbol{G}_{gg}(i\omega) = \begin{bmatrix} \boldsymbol{0} & \boldsymbol{0} \\ \boldsymbol{0} & \boldsymbol{G}_{hh}(i\omega) \end{bmatrix}; \quad \bar{\boldsymbol{f}}_g(i\omega) = \begin{Bmatrix} \boldsymbol{0} \\ \bar{\boldsymbol{f}}_h(i\omega) \end{Bmatrix} \tag{42.32}$$

Vector $\bar{\boldsymbol{f}}_h(i\omega)$ is the free-field soil "seismic driving force" vector defined by Eq. (42.15), in which the free-field soil displacements in vector $\bar{\boldsymbol{u}}_h(i\omega)$ result from scattering of incident seismic waves propagating to the bridge site as explained previously in Section 42.5.

Nonlinear Modeling

When large nonlinearities develop in the structure–foundation subsystem during a seismic event, evaluation of its performance requires nonlinear modeling and analysis in the time domain. In this case, the standard linear equations of motion of the complete system as expressed by

$$\begin{bmatrix} \boldsymbol{M}_{ss} & \boldsymbol{M}_{sf} & \boldsymbol{0} \\ \boldsymbol{M}_{sf}^T & \boldsymbol{M}_{ff} & \boldsymbol{M}_{fg} \\ \boldsymbol{0} & \boldsymbol{M}_{fg}^T & \boldsymbol{M}_{gg} \end{bmatrix} \begin{Bmatrix} \ddot{\boldsymbol{u}}_s(t) \\ \ddot{\boldsymbol{u}}_f(t) \\ \ddot{\boldsymbol{u}}_g(t) \end{Bmatrix} + \begin{bmatrix} \boldsymbol{C}_{ss} & \boldsymbol{C}_{sf} & \boldsymbol{0} \\ \boldsymbol{C}_{sf}^T & \boldsymbol{C}_{ff} & \boldsymbol{C}_{fg} \\ \boldsymbol{0} & \boldsymbol{C}_{fg}^T & \boldsymbol{C}_{gg} \end{bmatrix} \begin{Bmatrix} \dot{\boldsymbol{u}}_s(t) \\ \dot{\boldsymbol{u}}_f(t) \\ \dot{\boldsymbol{u}}_g(t) \end{Bmatrix} + \begin{bmatrix} \boldsymbol{K}_{ss} & \boldsymbol{K}_{sf} & \boldsymbol{0} \\ \boldsymbol{K}_{sf}^T & \boldsymbol{K}_{ff} & \boldsymbol{K}_{fg} \\ \boldsymbol{0} & \boldsymbol{K}_{fg}^T & \boldsymbol{K}_{gg} \end{bmatrix} \begin{Bmatrix} \boldsymbol{u}_s(t) \\ \boldsymbol{u}_f(t) \\ \boldsymbol{u}_g(t) \end{Bmatrix} = \begin{Bmatrix} \boldsymbol{0} \\ \boldsymbol{0} \\ \boldsymbol{f}_g(t) \end{Bmatrix} \tag{42.33}$$

must be modified appropriately to characterize the nonlinearities for use in a step-by-step numerical solution. Usually, it is the third term on the left-hand side of this equation that must be modified to represent the nonlinear hysteretic force–deformation behavior taking place in the individual finite

elements of the system. The second term in this equation, representing viscous damping forces, is usually retained in its linear form with the full viscous damping matrix $\boldsymbol{C}$ being expressed in the Rayleigh form

$$\boldsymbol{C} = \alpha_R \boldsymbol{M} + \beta_R \boldsymbol{K} \tag{42.34}$$

in which $\boldsymbol{M}$ and $\boldsymbol{K}$ are the full mass and elastic-stiffness matrices shown in Eq. (42.33) and α_R and β_R are constants assigned numerical values which will limit the modal damping ratios to levels within acceptable bounds over a range of modal frequencies dominating the seismic response.

For a time-domain solution of Eq. (42.33) in its modified nonlinear form, all parameters in the equation must be real (no imaginary parts) and frequency independent. It remains therefore to modify the soil impedance matrix $\boldsymbol{G}_{hh}(i\omega)$ so that when introduced into Eq. (42.30), the inverse Fourier transform of $-\boldsymbol{f}_h(i\omega)$ to the time domain will yield a vector $-\boldsymbol{f}_h(t)$ having no frequency-dependent parameters. To accomplish this objective, separate $\boldsymbol{G}_{hh}(i\omega)$ into its real and imaginary parts in accordance with

$$\boldsymbol{G}_{hh}(i\omega) = \boldsymbol{G}^R_{hh}(\omega) + i\boldsymbol{G}^I_{hh}(\omega) \tag{42.35}$$

in which $\boldsymbol{G}^R_{hh}(\omega)$ and $\boldsymbol{G}^I_{hh}(\omega)$ are real functions of ω. Then approximate these functions using the relations

$$\boldsymbol{G}^R_{hh}(\omega) \doteq \overline{\boldsymbol{K}}_{hh} - \omega^2 \overline{\boldsymbol{M}}_{hh}\,; \quad \boldsymbol{G}^I_{hh}(\omega) \doteq \omega \overline{\boldsymbol{C}}_{hh} \tag{42.36}$$

where the real constants in matrices $\overline{\boldsymbol{K}}_{hh}$, $\overline{\boldsymbol{M}}_{hh}$, and $\overline{\boldsymbol{C}}_{hh}$ are assigned numerical values to provide best fits to the individual frequency-dependent functions in matrices $\boldsymbol{G}^R_{hh}(\omega)$ and $\boldsymbol{G}^I_{hh}(\omega)$ over the frequency range of major influence on seismic response. Typically, applying these best fits to the range $0 < \omega < 4\pi$ radians/second, corresponding to the range $0 < f < 2$ Hz, where $f = \omega/2\pi$, is adequate for most large bridges. In this fitting process, it is sufficient to treat $\overline{\boldsymbol{M}}_{hh}$ as a diagonal matrix, thus affecting only the diagonal functions in matrix $\boldsymbol{G}^R_{hh}(\omega)$. The reason for selecting the particular frequency-dependent forms of Eqs. (42.36) is that when they are substituted into Eq. (42.35), which in turn is substituted into Eq. (42.30), the resulting expression for $\boldsymbol{f}_h(i\omega)$ can be Fourier transformed to the time domain yielding

$$-\boldsymbol{f}_h(t) = \overline{\boldsymbol{K}}_{hh}\left\{\overline{\boldsymbol{u}}_h(t) - \boldsymbol{u}_h(t)\right\} + \overline{\boldsymbol{C}}_{hh}\left\{\dot{\overline{\boldsymbol{u}}}_h(t) - \dot{\boldsymbol{u}}_h(t)\right\} + \overline{\boldsymbol{M}}_{hh}\left\{\ddot{\overline{\boldsymbol{u}}}_h(t) - \ddot{\boldsymbol{u}}_h(t)\right\} \tag{42.37}$$

Substituting $-\boldsymbol{f}_h(t)$ given by this equation for the last h components in vector $\boldsymbol{f}_g(t)$, with all other components in $\boldsymbol{f}_g(t)$ being equal to zero, and then substituting the resulting vector $\boldsymbol{f}_g(t)$ into Eq. (42.33) gives

$$\begin{bmatrix} \boldsymbol{M}_{ss} & \boldsymbol{M}_{sf} & \boldsymbol{0} \\ \boldsymbol{M}^T_{sf} & \boldsymbol{M}_{ff} & \boldsymbol{M}_{fg} \\ \boldsymbol{0} & \boldsymbol{M}^T_{fg} & [\boldsymbol{M}_{gg} + \overline{\boldsymbol{M}}_{gg}] \end{bmatrix} \begin{Bmatrix} \ddot{\boldsymbol{u}}_s(t) \\ \ddot{\boldsymbol{u}}_f(t) \\ \ddot{\boldsymbol{u}}_g(t) \end{Bmatrix} + \begin{bmatrix} \boldsymbol{C}_{ss} & \boldsymbol{C}_{sf} & \boldsymbol{0} \\ \boldsymbol{C}^T_{sf} & \boldsymbol{C}_{ff} & \boldsymbol{C}_{fg} \\ \boldsymbol{0} & \boldsymbol{C}^T_{fg} & [\boldsymbol{C}_{gg} + \overline{\boldsymbol{C}}_{gg}] \end{bmatrix} \begin{Bmatrix} \dot{\boldsymbol{u}}_s(t) \\ \dot{\boldsymbol{u}}_f(t) \\ \dot{\boldsymbol{u}}_g(t) \end{Bmatrix} + \tag{42.38}$$

$$\begin{bmatrix} \boldsymbol{K}_{ss} & \boldsymbol{K}_{sf} & \boldsymbol{0} \\ \boldsymbol{K}^T_{sf} & \boldsymbol{K}_{ff} & \boldsymbol{K}_{fg} \\ \boldsymbol{0} & \boldsymbol{K}^T_{fg} & [\boldsymbol{K}_{gg} + \overline{\boldsymbol{K}}_{gg}] \end{bmatrix} \begin{Bmatrix} \boldsymbol{u}_s(t) \\ \boldsymbol{u}_f(t) \\ \boldsymbol{u}_g(t) \end{Bmatrix} = \begin{Bmatrix} \boldsymbol{0} \\ \boldsymbol{0} \\ \overline{\boldsymbol{K}}_{gg}\overline{\boldsymbol{u}}_g(t) + \overline{\boldsymbol{C}}_{gg}\dot{\overline{\boldsymbol{u}}}_g(t) + \overline{\boldsymbol{M}}_{gg}\ddot{\overline{\boldsymbol{u}}}_g(t) \end{Bmatrix}$$

in which

$$\overline{\boldsymbol{M}}_{gg} = \begin{bmatrix} \mathbf{0} & \mathbf{0} \\ \mathbf{0} & \overline{\boldsymbol{M}}_{hh} \end{bmatrix}; \quad \overline{\boldsymbol{K}}_{gg} = \begin{bmatrix} \mathbf{0} & \mathbf{0} \\ \mathbf{0} & \overline{\boldsymbol{K}}_{hh} \end{bmatrix}; \quad \overline{\boldsymbol{C}}_{gg} = \begin{bmatrix} \mathbf{0} & \mathbf{0} \\ \mathbf{0} & \overline{\boldsymbol{C}}_{hh} \end{bmatrix} \tag{42.39}$$

showing that no frequency-dependent parameters remain in the equations of motion, thus allowing the standard time-domain solution procedure to be used for solving them. Usually, the terms $\overline{\boldsymbol{C}}_{gg}\,\dot{\boldsymbol{u}}_g(t)$ and $\overline{\boldsymbol{M}}_{gg}\,\ddot{\boldsymbol{u}}_g(t)$ on the right-hand side of Eq. (42.38) have small effects on the solution of this equation; however, the importance of their contributions should be checked. Having modified the third term on the left-hand side of Eq. (42.38) to its nonlinear hysteretic form, the complete set of coupled equations can be solved for displacements $\boldsymbol{u}_s(t)$, $\boldsymbol{u}_f(t)$, $\boldsymbol{u}_g(t)$ using standard step-by-step numerical integration procedures.

42.6.2 Solution Procedures

One-Step Direct Approach

In this approach, the equations of motion are solved directly in their coupled form. If the system is treated as being fully linear (or equivalent linear), the solution can be carried out in the frequency domain using Eq. (42.31). In doing so, the complete set of complex algebraic equations is solved separately for discrete values of ω over the frequency range of interest yielding the corresponding sets of displacement vectors $\boldsymbol{u}_s(i\omega)$, $\boldsymbol{u}_f(i\omega)$, and $\boldsymbol{u}_g(i\omega)$. Having obtained these vectors for the discrete values of ω, they are inverse Fourier transformed to the time domain giving vectors $\boldsymbol{u}_s(t)$, $\boldsymbol{u}_f(t)$, $\boldsymbol{u}_g(t)$. The corresponding time histories of internal forces and/or deformations in the system can then be obtained directly using standard finite-element procedures.

If the structure–foundation subsystem is modeled as a nonlinear system, the solution can be carried out in the time domain using Eq. (42.38). In this case, the coupled nonlinear equations of motion are solved using standard step-by-step numerical integration procedures.

This one-step direct approach is simple and straightforward to implement for a structural system supported on a single foundation, such as a building. However, for a long, multiple-span bridge supported on many independent foundations, a very large system of equations and an associated very large number of seismic free-field inputs in vector $\overline{\boldsymbol{u}}_g\ (i\omega)$ result, making the solution computationally impractical, especially when large nonlinearities are present in the equations of motion. In this case, it is desirable to simplify the problem by finding separate solutions to a set of smaller problems and then combine the solutions in steps so as to achieve the desired end result. The multiple-step substructuring approach described subsequently is ideally suited for this purpose.

Multiple-Step Substructuring Approach

For long bridges supported on multiple foundations, the support separation distances are sufficiently large so that each foundation subsystem can be treated as being independent of the others; therefore, the soil impedance matrix for each foundation will be uncoupled from those of the other foundations. In this case, to simplify the overall problem, each foundation subsystem can be analyzed separately to obtain a boundary impedance matrix called the foundation impedance matrix and a consistent boundary force vector called the foundation driving-force vector, both of which are associated with the DOF at its structure–foundation interface. Having obtained the foundation impedance matrix and associated driving force vector for each foundation subsystem, all such matrices and vectors can be combined into the equations of motion for the total structure as a free-free system, resulting in $(s + f)$ DOF present in the structure–foundation subsystem rather than the $(s + f + g)$ DOF present in the complete soil–structure–foundation system. This reduced set of equations having $(s + f)$ DOF can be solved much more efficiently than solving the equations for the complete system having $(s + f + g)$ DOF as required by the one-step direct approach.

Referring to Eq. (42.31), it is seen that the linear equations of motion for each independent foundation system j can be expressed in the frequency-domain form:

$$\begin{bmatrix} \boldsymbol{D}_{ff}^{j}(i\omega) & \boldsymbol{D}_{fg}^{j}(i\omega) \\ \boldsymbol{D}_{fg}^{j}(i\omega)^{T} & [\boldsymbol{D}_{gg}^{j}(i\omega)+\boldsymbol{G}_{gg}^{j}(i\omega)] \end{bmatrix} \begin{Bmatrix} \boldsymbol{u}_{f}^{j}(i\omega) \\ \boldsymbol{u}_{g}^{j}(i\omega) \end{Bmatrix} = \begin{Bmatrix} \boldsymbol{0} \\ \overline{\boldsymbol{f}}_{g}^{j}(i\omega) \end{Bmatrix} \tag{42.40}$$

in which

$$\overline{\boldsymbol{f}}_{g}^{j}(i\omega) = \boldsymbol{G}_{gg}^{j}(i\omega)\overline{\boldsymbol{u}}_{g}^{j}(i\omega) \tag{42.41}$$

Solving the second of Eqs. (42.40) for $\boldsymbol{u}_{g}^{j}(i\omega)$ gives

$$\boldsymbol{u}_{g}^{j}(i\omega) = \left[\boldsymbol{D}_{gg}^{j}(i\omega)+\boldsymbol{G}_{gg}^{j}(i\omega)\right]^{-1}\left[-\boldsymbol{D}_{fg}^{j}(i\omega)^{T}\boldsymbol{u}_{f}^{j}(i\omega)+\overline{\boldsymbol{f}}_{g}^{j}(i\omega)\right] \tag{42.42}$$

Substituting this equation into the first of Eqs. (42.40) yields

$$\left[\boldsymbol{D}_{ff}^{j}(i\omega)+\boldsymbol{F}_{ff}^{j}(i\omega)\right]\boldsymbol{u}_{f}^{j}(i\omega) = \overline{\boldsymbol{f}}_{f}^{j}(i\omega) \tag{42.43}$$

where

$$\boldsymbol{F}_{ff}^{j}(i\omega) \equiv -\boldsymbol{D}_{fg}^{j}(i\omega)[\boldsymbol{D}_{gg}^{j}(i\omega)+\boldsymbol{G}_{gg}^{j}(i\omega)]^{-1}\boldsymbol{D}_{fg}^{j}(i\omega)^{T} \tag{42.44}$$

$$\overline{\boldsymbol{f}}_{f}^{j}(i\omega) \equiv -\boldsymbol{D}_{fg}^{j}(i\omega)[\boldsymbol{D}_{gg}^{j}(i\omega)+\boldsymbol{G}_{gg}^{j}(i\omega)]^{-1}\overline{\boldsymbol{f}}_{g}^{j}(i\omega) \tag{42.45}$$

Matrix $\boldsymbol{F}_{ff}^{j}(i\omega)$ and vector $\overline{\boldsymbol{f}}_{f}^{j}(i\omega)$ will be referred to here as the foundation impedance matrix and its associated foundation driving-force vector, respectively, for the jth foundation. For convenience, a foundation motion vector $\overline{\boldsymbol{u}}_{f}^{j}(i\omega)$ will now be defined as given by

$$\overline{\boldsymbol{u}}_{f}^{j}(i\omega) \equiv \boldsymbol{F}_{ff}^{j}(i\omega)^{-1}\overline{\boldsymbol{f}}_{f}^{j}(i\omega) \tag{42.46}$$

so that the driving-force vector $\overline{\boldsymbol{f}}_{f}^{j}(i\omega)$ can be expressed in the form

$$\overline{\boldsymbol{f}}_{f}^{j}(i\omega) = \boldsymbol{F}_{ff}^{j}(i\omega)\overline{\boldsymbol{u}}_{f}^{j}(i\omega) \tag{42.47}$$

The motion vector $\overline{\boldsymbol{u}}_{f}^{j}(i\omega)$ given by Eq. (42.46) will be referred to subsequently as the "effective (scattered) foundation input motion" vector. Conceptually, this is the vector of foundation motions which, when multiplied by the foundation impedance matrix $\boldsymbol{F}_{ff}^{j}(i\omega)$, yields the foundation driving-force vector $\overline{\boldsymbol{f}}_{f}^{j}(i\omega)$ resulting from the prescribed scattered free-field soil input motions contained in vector $\overline{\boldsymbol{u}}_{g}^{j}(i\omega)$.

Combining Eqs. (42.43) for all foundation subsystems with the equations of motion for the complete free-free structure subsystem yields the desired reduced matrix equation of motion for the entire structure–foundation system in the linear form

$$\begin{bmatrix} \boldsymbol{D}_{ss}(i\omega) & \boldsymbol{D}_{sf}(i\omega) \\ \boldsymbol{D}_{sf}(i\omega)^{T} & [\boldsymbol{D}_{ff}^{s}(i\omega)+\boldsymbol{F}_{ff}(i\omega)] \end{bmatrix} \begin{Bmatrix} \boldsymbol{u}_{s}(i\omega) \\ \boldsymbol{u}_{f}(i\omega) \end{Bmatrix} = \begin{Bmatrix} \boldsymbol{0} \\ \overline{\boldsymbol{f}}_{f}(i\omega) \end{Bmatrix} \tag{42.48}$$

in which $\boldsymbol{D}_{ss}(i\omega)$ and $\boldsymbol{D}_{sf}(i\omega)$ are given by Eqs. (42.27) and (42.28) directly, $\boldsymbol{D}^{s}_{ff}(i\omega)$ is that part of $\boldsymbol{D}_{ff}(i\omega)$ given by these same equations as contributed by the structure only, and

$$\overline{\boldsymbol{f}}_f(i\omega) = \boldsymbol{F}_{ff}(i\omega)\overline{\boldsymbol{u}}_f(i\omega) \tag{42.49}$$

The solution of Eq. (42.48) for discrete values of ω over the frequency range of interest gives the desired solutions for $\boldsymbol{u}_s(i\omega)$ and $\boldsymbol{u}_f(i\omega)$. To obtain the corresponding solution $\boldsymbol{u}^j_g(i\omega)$ for each foundation subsystem *j*, a backsubstitution is required. This is done by substituting the solution $\boldsymbol{u}^j_f(i\omega)$ for each foundation subsystem *j* into Eq. (42.42) and computing the corresponding response motions in vector $\boldsymbol{u}^j_g(i\omega)$. This step will be called the "foundation feedback" analysis.

When large nonlinearities develop in the structure during a seismic event, the reduced equations of motion representing the coupled structure–foundation system must be expressed in the time domain. To do so, consider the structure alone as a free-free linear system having externally applied forces $\boldsymbol{f}_f(t)$ acting in the *f* DOF. The equations of motion for this system can be expressed in the frequency domain form:

$$\begin{bmatrix} \boldsymbol{D}_{ss}(i\omega) & \boldsymbol{D}_{sf}(i\omega) \\ \boldsymbol{D}_{sf}(i\omega)^T & \boldsymbol{D}^s_{ff}(i\omega) \end{bmatrix} \begin{Bmatrix} \boldsymbol{u}_s(i\omega) \\ \boldsymbol{u}_f(i\omega) \end{Bmatrix} = \begin{Bmatrix} \boldsymbol{0} \\ \boldsymbol{f}_f(i\omega) \end{Bmatrix} \tag{42.50}$$

in which $\boldsymbol{f}_f(i\omega)$ is the Fourier transform of vector $\boldsymbol{f}_f(t)$. If Eq. (42.50) is to represent the coupled structure–foundation system, then $\boldsymbol{f}_f(i\omega)$ must satisfy the relation

$$\boldsymbol{f}_f(i\omega) = \boldsymbol{F}_{ff}(i\omega)\left\{\overline{\boldsymbol{u}}_f(i\omega) - \boldsymbol{u}_f(i\omega)\right\} \tag{42.51}$$

in which matrix $\boldsymbol{F}_{ff}(i\omega)$ is an assembly of the individual foundation impedance matrices $\boldsymbol{F}^j_{ff}(i\omega)$ given by Eq. (42.44) for all values of *j* and vector $\overline{\boldsymbol{u}}_f(i\omega)$ is the corresponding complete foundation-motion vector containing all individual vectors $\overline{\boldsymbol{u}}^j_f(i\omega)$ given by Eq. (42.46).

Equation (42.50) can be converted to the time-domain form:

$$\begin{bmatrix} \boldsymbol{M}_{ss} & \boldsymbol{M}_{sf} \\ \boldsymbol{M}^T_{sf} & \boldsymbol{M}^s_{ff} \end{bmatrix} \begin{Bmatrix} \ddot{\boldsymbol{u}}_s(t) \\ \ddot{\boldsymbol{u}}_f(t) \end{Bmatrix} + \begin{bmatrix} \boldsymbol{C}_{ss} & \boldsymbol{C}_{sf} \\ \boldsymbol{C}^T_{sf} & \boldsymbol{C}^s_{ff} \end{bmatrix} \begin{Bmatrix} \dot{\boldsymbol{u}}_s(t) \\ \dot{\boldsymbol{u}}_f(t) \end{Bmatrix} + \begin{bmatrix} \boldsymbol{K}_{ss} & \boldsymbol{K}_{sf} \\ \boldsymbol{K}^T_{sf} & \boldsymbol{K}^s_{ff} \end{bmatrix} \begin{Bmatrix} \boldsymbol{u}_s(t) \\ \boldsymbol{u}_f(t) \end{Bmatrix} = \begin{Bmatrix} \boldsymbol{0} \\ \boldsymbol{f}_f(t) \end{Bmatrix} \tag{42.52}$$

in which $\boldsymbol{K}^s_{ff}$, $\boldsymbol{C}^s_{ff}$, and $\boldsymbol{M}^s_{ff}$ are the standard stiffness, damping, and mass matrices contributed by the structure only (no contributions from the foundation) and $\boldsymbol{f}_f(t)$ is the inverse Fourier transform of $\boldsymbol{f}_f(i\omega)$ given by Eq. (42.51). In order for $\boldsymbol{f}_f(t)$ to have no frequency-dependent parameters, as required by a time-domain solution, matrix $\mathbf{F}_{ff}(i\omega)$ should be separated into its real and imaginary parts in accordance with

$$\boldsymbol{F}_{ff}(i\omega) = \boldsymbol{F}^R_{ff}(\omega) + \boldsymbol{i}\boldsymbol{F}^I_{ff}(\omega) \tag{42.53}$$

in which $\boldsymbol{F}^R_{ff}(\omega)$ and $\boldsymbol{F}^I_{ff}(\omega)$ can be approximated using the relations

$$\boldsymbol{F}^R_{ff}(\omega) \doteq (\overline{\boldsymbol{K}}_{ff} - \omega^2\overline{\boldsymbol{M}}_{ff}); \quad \boldsymbol{F}^I_{ff}(\omega) \doteq \omega\overline{\boldsymbol{C}}_{ff} \tag{42.54}$$

where the real constants in matrices $\overline{\boldsymbol{K}}_{ff}$, $\overline{\boldsymbol{M}}_{ff}$, and $\overline{\boldsymbol{C}}_{ff}$ are assigned numerical values to provide best fits to the individual frequency-dependent functions in matrices $\boldsymbol{F}^R_{ff}(\omega)$ and $\boldsymbol{F}^I_{ff}(\omega)$ over the frequency range of major influence on seismic response; usually the range $0 < \omega < 4\pi$ rad/s. is adequate for large bridges. In this fitting process, it is sufficient to treat $\overline{\boldsymbol{M}}_{ff}$ as a diagonal matrix, thus affecting only the diagonal functions in matrix $\boldsymbol{F}^R_{ff}(\omega)$.

Substituting Eqs. (42.54) into Eq. (42.53) and the resulting Eq. (42.53) into Eq. (42.51), this latter equation can be inverse Fourier transformed, giving

$$f_t(t) = \overline{K}_{ff}\left\{\overline{u}_f(t) - u_f(t)\right\} + \overline{C}_{ff}\left\{\dot{\overline{u}}_f(t) - \dot{u}_f(t)\right\} + \overline{M}_{ff}\left\{\ddot{\overline{u}}_f(t) - \ddot{u}_f(t)\right\} \tag{42.55}$$

which when introduced into Eq. (42.50) yields the desired reduced linear equations of motion in the time-domain form

$$\begin{bmatrix} \boldsymbol{M}_{ss} & \boldsymbol{M}_{ff} \\ \boldsymbol{M}_{sf}^T & [\boldsymbol{M}_{ff}^s + \overline{\boldsymbol{M}}_{ff}] \end{bmatrix} \begin{Bmatrix} \ddot{\boldsymbol{u}}_s(t) \\ \ddot{\boldsymbol{u}}_f(t) \end{Bmatrix} + \begin{bmatrix} \boldsymbol{C}_{ss} & \boldsymbol{C}_{sf} \\ \boldsymbol{C}_{sf}^T & [\boldsymbol{C}_{ff}^s + \overline{\boldsymbol{C}}_{ff}] \end{bmatrix} \begin{Bmatrix} \dot{\boldsymbol{u}}_s(t) \\ \dot{\boldsymbol{u}}_f(t) \end{Bmatrix} +$$

$$\begin{bmatrix} \boldsymbol{K}_{ss} & \boldsymbol{K}_{sf} \\ \boldsymbol{K}_{sf}^T & [\boldsymbol{K}_{ff}^s + \overline{\boldsymbol{K}}_{ff}] \end{bmatrix} \begin{Bmatrix} \boldsymbol{u}_s(t) \\ \boldsymbol{u}_f(t) \end{Bmatrix} = \begin{bmatrix} \boldsymbol{0} \\ \overline{\boldsymbol{K}}_{ff}\overline{\boldsymbol{u}}_{\boldsymbol{f}}(t) + \overline{\boldsymbol{C}}_{ff}\dot{\overline{\boldsymbol{u}}}_{\boldsymbol{f}}(t) + \overline{\boldsymbol{M}}_{ff}\ddot{\overline{\boldsymbol{u}}}_{\boldsymbol{f}}(t) \end{bmatrix} \tag{42.56}$$

showing that no frequency-dependent parameters remain in the equations of motion, thus satisfying the time-domain solution requirement. Again, as explained previously, the full viscous damping matrix in this equation is usually expressed in the Rayleigh form given by Eq. (42.34) in which constants α_R and β_R are assigned numerical values to limit the modal damping ratios to levels within acceptable bounds over the range of frequencies dominating seismic response. As explained previously for Eq. (42.38), the damping and mass terms on the right-hand side of Eq. (42.56) usually have small effects on the solution; however, their importance should be checked.

Having modified the third term on the left-hand side of Eq. (42.56) to its nonlinear hysteretic form, the complete set of coupled equations can be solved for displacements $\boldsymbol{u}_s(t)$ and $\boldsymbol{u}_f(t)$ using standard step-by-step numerical integration procedures.

To obtain the corresponding $\boldsymbol{u}_g^j(i\omega)$ for each foundation subsystem *j*, the previously defined foundation feedback analyses must be performed. To do so, each subvector $\boldsymbol{u}_f^j(t)$ contained in vector $\boldsymbol{u}_f(t)$, must be Fourier transformed to obtain $\boldsymbol{u}_f^j(i\omega)$. Having these subvectors for all values of *j*, each one can be substituted separately into Eq. (42.42) giving the corresponding subvector $\boldsymbol{u}_g^j(i\omega)$. Inverse Fourier transforming each of these subvectors yields the corresponding vectors $\boldsymbol{u}_f^j(t)$ for all values of *j*.

42.7 Demand Analysis Examples

This section presents the results of three example solutions to illustrate applications of the demand analysis procedures described in the previous section, in particular, the multiple-step substructuring approach. These examples have been chosen from actual situations to illustrate application of the three methods of soil–foundation modeling: (1) the elastodynamic method, (2) the empirical *p–y* method, and (3) the hybrid method.

42.7.1 Caisson Foundation

The first example is chosen to illustrate application of the elastodynamic method of modeling and analysis to a deeply embedded caisson foundation of a large San Francisco Bay crossing bridge. The foundation considered is a large reinforced concrete cellular caisson, 80 ft (24.4 m) long, 176 ft (53.6 m) wide, and 282 ft (86.0 m) tall, located at a deep soil site and filled with water. The configuration of the caisson and its supporting soil profile and properties are shown in Figure 42.8. The soil properties are the shear-strain-compatible equivalent linear properties obtained from free-field site-response analyses using SHAKE with the seismic input motions prescribed at the bedrock surface

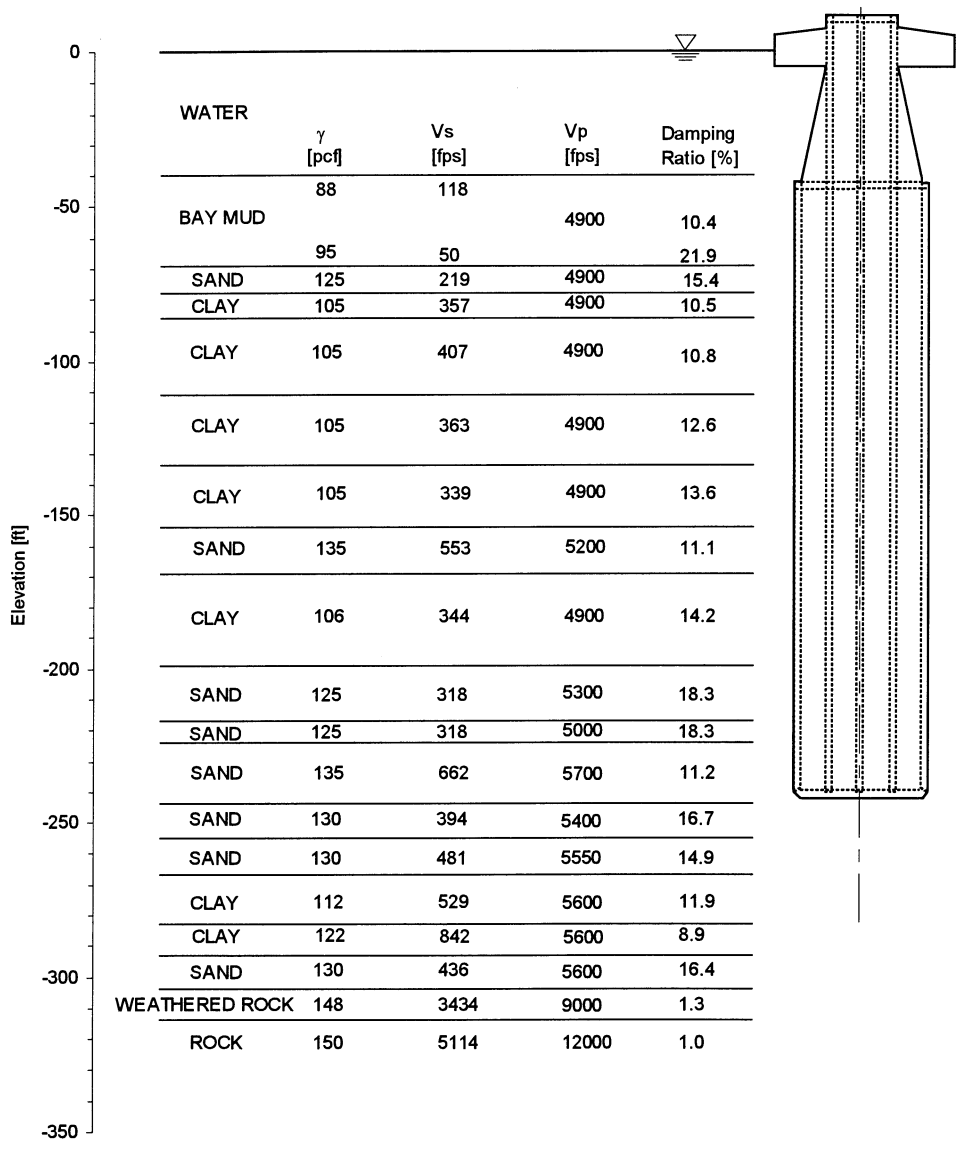

FIGURE 42.8 Configuration and soil profile and properties of the cassion foundation at its SASSI half-model.

in the form of rock-outcrop motion. Thus, these properties have incorporated stiffness degradation effects due to global soil nonlinearities induced in the free-field by the selected seismic input.

Since the caisson is deeply embedded and has large horizontal dimensions, the local soil nonlinearities that develop near the soil–caisson interface are relatively small; therefore, they were neglected in the demand analysis. The soil–caisson system was modeled using the elastodynamic method; i.e., the system was modeled by an elastic foundation structure embedded in a damped-elastic soil medium having the properties shown in Figure 42.8. This model, developed using the finite-element SASSI computer program for one quarter of the soil–caisson system, is shown in Figure 42.8. Using this model, the foundation impedance matrix, i.e., $\boldsymbol{F}_{ff}^{j}(i\omega)$ defined by Eq. (42.44), and its associated effective (scattered) foundation input motion vector, i.e., $\bar{\boldsymbol{u}}_{f}^{j}(i\omega)$ defined by Eq. (42.46), were evaluated consistent with the free-field seismic input using SASSI. The foundation impedance matrix associated with the six DOF of the node located at the top of the caisson El. 40 ft. (12.2 m) was

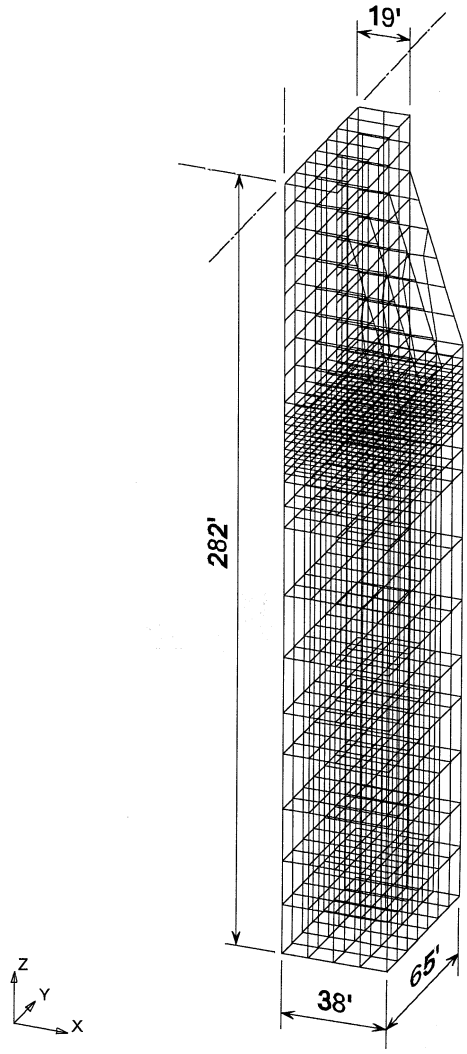

FIGURE 42.8 (continued)

computed following the procedure described in Section 42.6. The individual impedance functions in this matrix are shown in Figure 42.9. The amplitudes of the transfer functions for longitudinal response motions of the caisson relative to the corresponding seismic input motion, as computed for several elevations, are shown in Figure 42.10. The 5% damped acceleration response spectra computed for these motions are also shown in Figure 42.10 where they can be compared with the 5% damped response spectra for the corresponding seismic input motion prescribed at the bedrock level and the corresponding free-field soil motion at the mudline elevation.

As indicated in Figure 42.10, the soil–caisson interaction system alone, without pier tower and superstructure of the bridge being present, has characteristic translational and rocking mode frequencies of 0.7 and 1.4 Hz (periods 1.4 and 0.7 s), respectively. The longitudinal scattered foundation motion associated with the foundation impedance matrix mentioned above is the motion represented by the response spectrum for El. 40 ft (12.2 m) as shown in Figure 42.10.

The response spectra shown in Figure 42.10 indicate that, because of the 0.7-s translational period of the soil–caisson system, the scattered foundation motion at the top of the caisson where the bridge pier tower would be supported, exhibits substantial amplifications in the neighborhood of

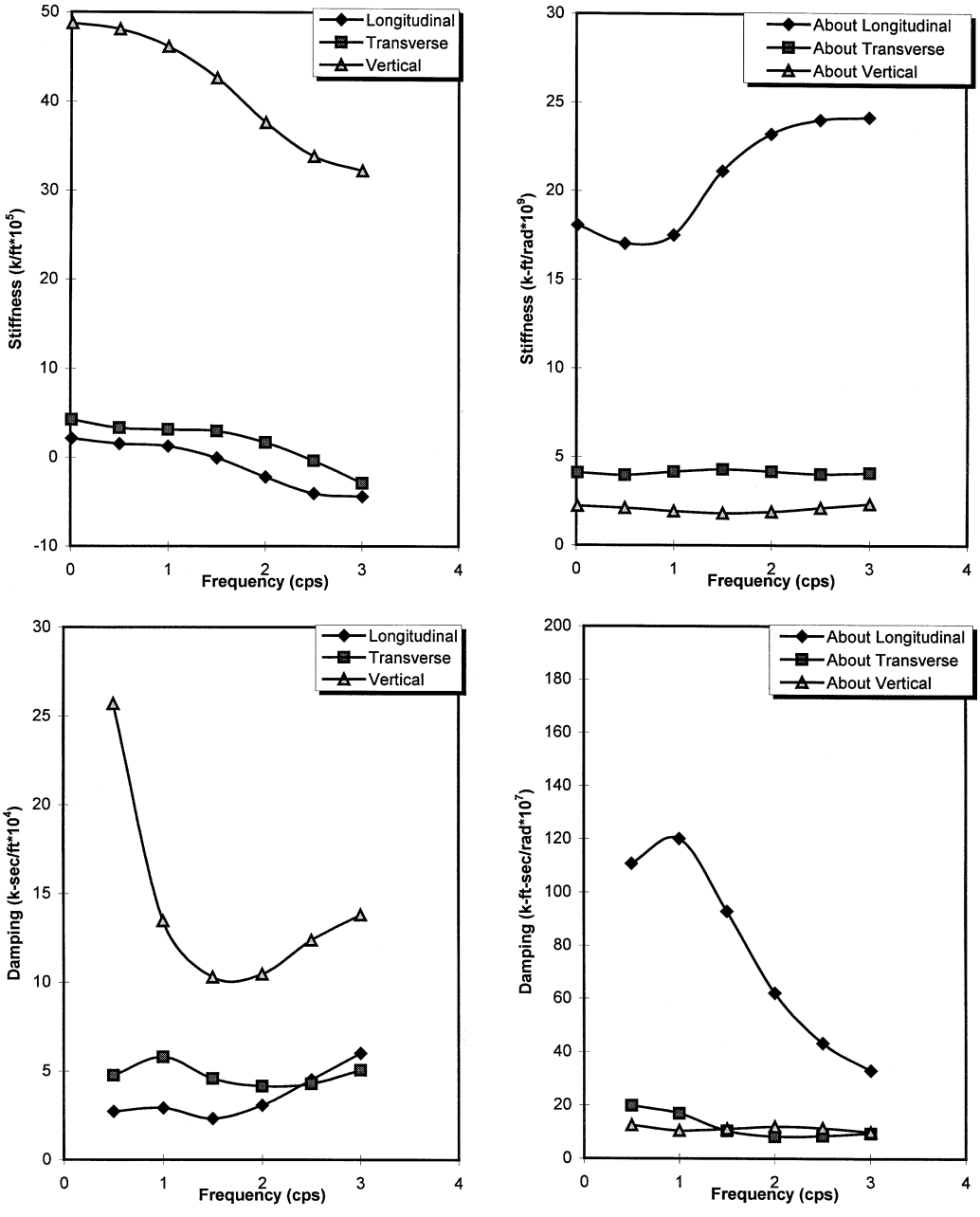

FIGURE 42.9 Foundation impedance functions at the top of the caisson considered.

this period. In the period range longer than 2.0 s, in which the major natural vibration frequencies of the bridge system are located, the spectral values for the scattered foundation input motion are seen to be smaller than the corresponding values for the free-field mudline motion. The above results point out the importance of properly modeling both the stiffness and the inertial properties of the soil–caisson system so that the resulting scattered foundation motions to be used as input to the foundation–structure system will appropriately represent the actual dynamic characteristics of the soil–caisson interaction system.

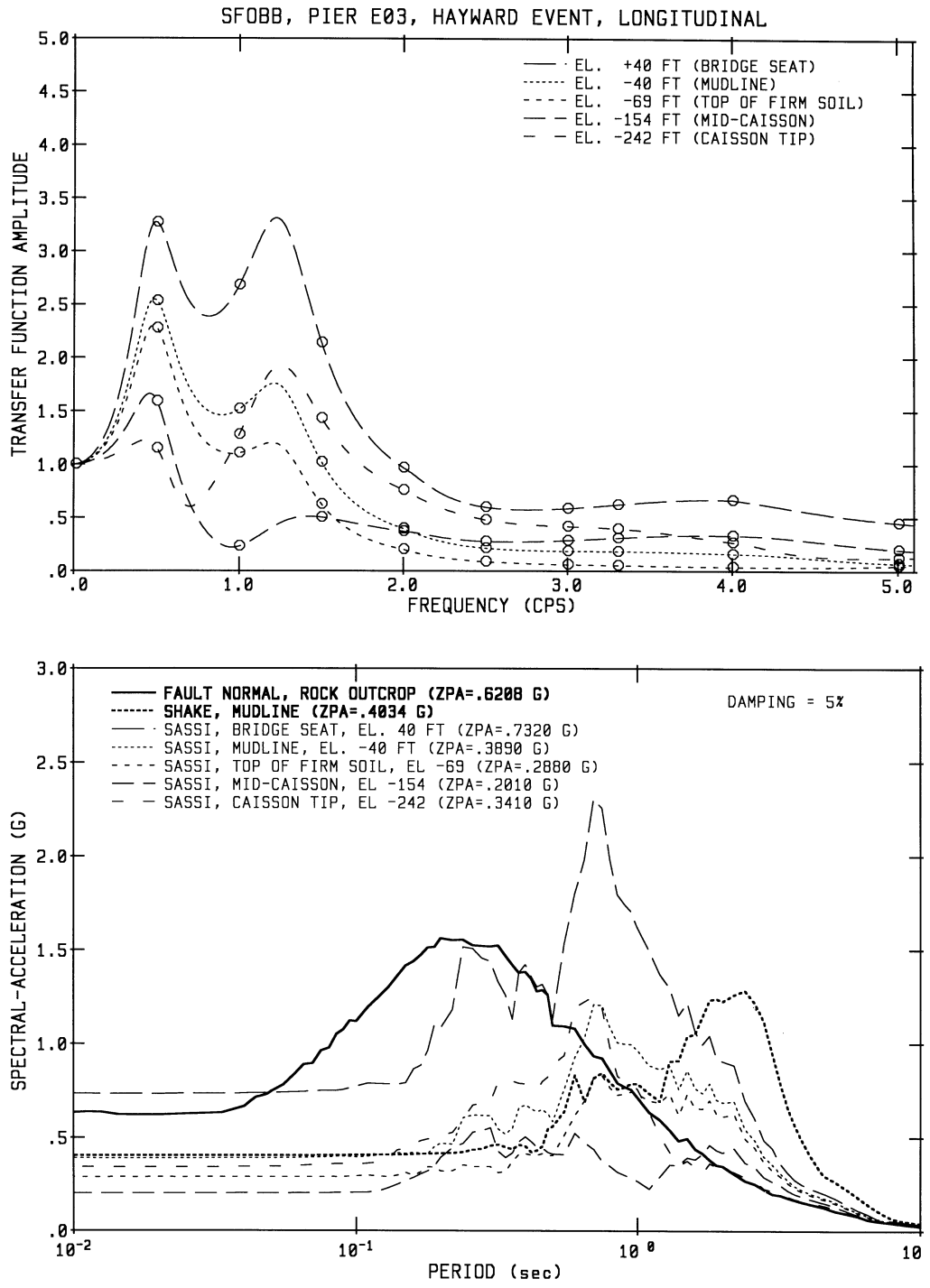

FIGURE 42.10 Transfer function amplitudes and 5% damped response spectra for scattered foundation motions of the caisson at several elevations.

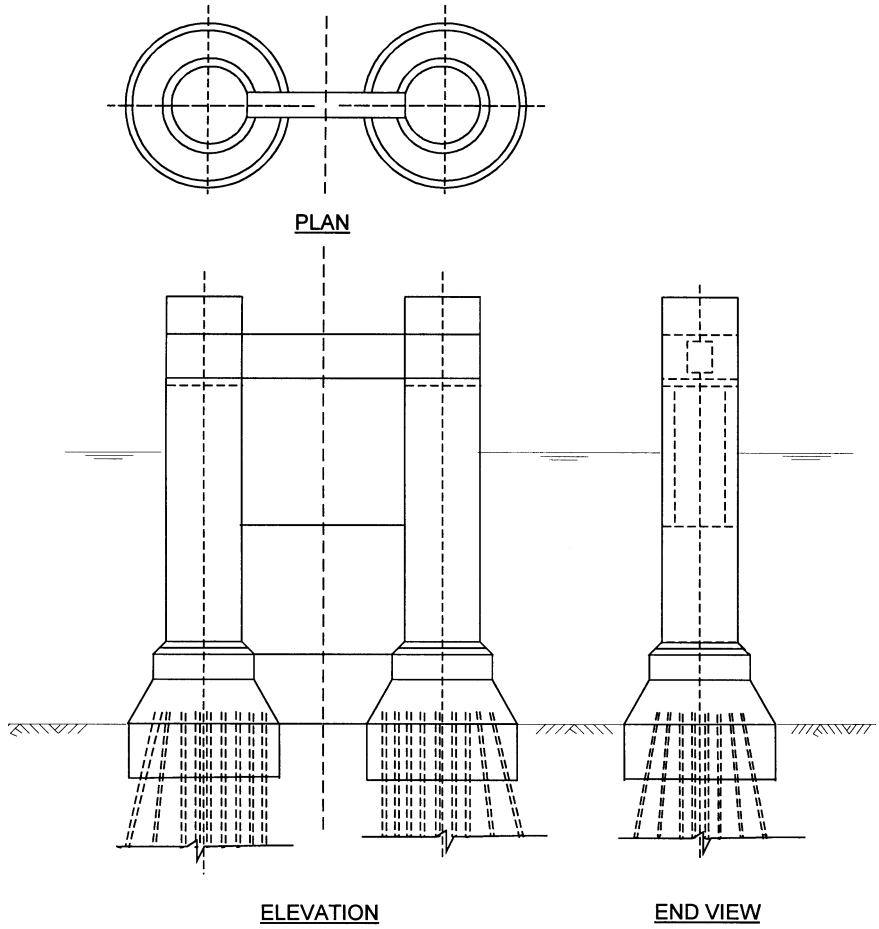

FIGURE 42.11 Configuration of the slender-pile group foundation considered.

42.7.2 Slender-Pile Group Foundation

The second example is to illustrate application of the empirical *p–y* method in a demand analysis of a slender-pile group foundation constructed at a deep soil site. The pile group foundation selected is one of 78 pier foundations of a long, water-crossing steel truss bridge. The foundation is constructed of two 24-ft (7.32-m)-diameter bell-shaped precast reinforced concrete pile caps, which are linked together by a deep cross-beam, as shown in Figure 42.11. Each bell-shaped pile cap is supported on a group of 28 steel 14BP89 H-pipes, giving a total of 56 piles supporting the combined two-bell pile cap. The piles in the outer ring and in the adjacent inner ring are battered at an angle of 4 to 1 and 6 to 1, respectively, leaving the remaining piles as vertical piles. The top ends of all piles are embedded with sufficient lengths into the concrete that fills the interior space of the bell-shaped pile caps such that these piles can be considered as fixed-head piles. The piles penetrate deep into the supporting soil medium to an average depth of 147 ft (44.8 m) below the mudline, where they encounter a thick dense sand layer. The soil profile and properties at this foundation location are shown in Figure 42.12. As indicated in this figure, the top 55 ft (16.8 m) of the site soil is composed of a 35-ft (10.7-m) layer of soft bay mud overlying a 20-ft (6.1-m) layer of loose silty sand.

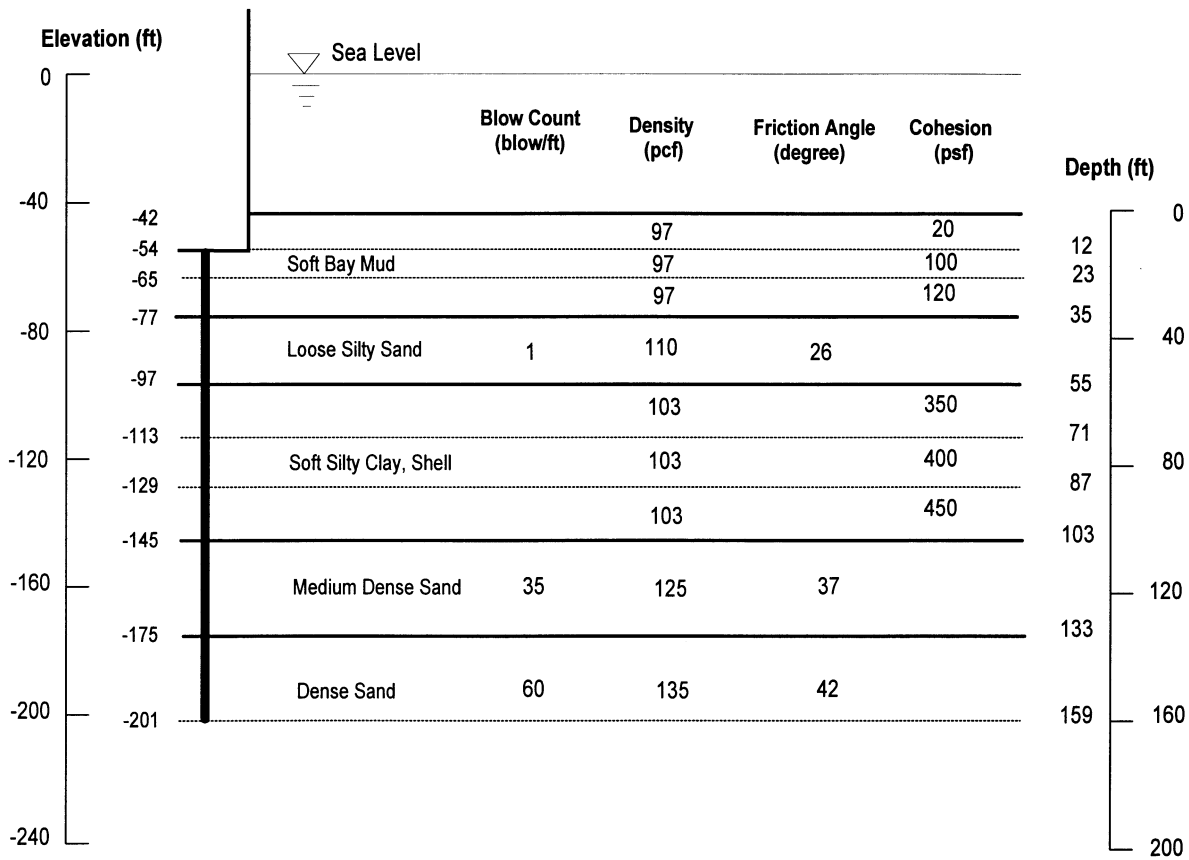

FIGURE 42.12 Soil profile and properties at the slender-pile group foundation considered.

Because of the soft topsoil layers and the slender piles used, the foundation under seismic excitations is expected to undergo relatively large foundation lateral displacements relative to the free-field soil. Thus, large local soil nonlinearities are expected to occur at the soil–pile interfaces. To model the nonlinear soil resistances to the lateral and axial deflections of the piles, the empirically derived lateral *p–y* and axial *t–z*, and the pile-tip *Q–d* curves for each pile were used. Typical *p–y* and *t–z* curves developed for the piles are shown in Figure 42.13. Using the nonlinear *p–y*, *t–z*, and *Q–d* curves developed, evaluation of the foundation impedance matrix, $\boldsymbol{F}_{ff}^{f}(i\omega)$, and the associated scattered foundation input motion vector, $\bar{\boldsymbol{u}}_f(i\omega)$, were obtained following the procedures described below:

1. Determine the pile group deflected shape using a nonlinear analysis program such as GROUP [52], LPIPE [53], and APILE2 [54], as appropriate, under an applied set of monotonically increasing axial and lateral forces and an overturning moment.
2. Select target levels of axial and lateral deflections at each selected soil depth corresponding to a selected target level of pile cap displacement and determine the corresponding secant moduli from the applicable nonlinear *p–y*, *t–z*, and *Q–d* curves.
3. Develop a model of a group of elastic beams supported on elastic axial and lateral soil springs for the pile group using the elastic properties of the piles and the secant moduli of the soil resistances obtained in Step 2 above.
4. Compute the foundation impedance matrix and associated scattered foundation input motion vector for the model developed in Step 3 using Eqs. (42.44) and (42.46).

Since the *p–y*, *t–z*, and *Q–d* curves represent pseudo-static force–deflection relations, the resulting foundation impedance matrix computed by the above procedure is a real (not complex) frequency-independent pseudo-static stiffness matrix, i.e., $\boldsymbol{F}_{ff}^{j}(i\omega) = \boldsymbol{F}_{ff}^{j}(0)$. For the pile group foundation considered in this example, the beam-on-elastic-spring model shown schematically in Figure 42.14 was used. The foundation stiffness matrix is associated with the six DOF of the nodal point located at the bottom center of the pile cap is shown in Figure 42.14. The scattered foundation motions in the longitudinal, transverse, and vertical directions associated with this foundation stiffness matrix are represented by their 5% damped acceleration response spectra shown in Figure 42.15. These spectra can be compared with the corresponding spectra for the seismic input motion prescribed at the pile tip elevation and the free-field mudline motions computed from free-field site-response analyses using SHAKE. As shown in Figure 42.15, the spectral values for the scattered pile cap motions, which would be used as input to the foundation–structure system, are lower than the spectral values for the free-field mudline motions. This result is to be expected for two reasons: (1) the soft topsoil layers present at the site are not capable of driving the pile group foundation and (2) the battered piles, acting with the vertical piles, resist lateral loads primarily through stiff axial truss action, in which case, the effective input motions at the pile cap are controlled more by the free-field soil motions at depth, where more competent soil resistances are present, than by the soil motions near the surface.

42.7.3 Large-Diameter Shaft Foundation

The third example illustrates the application of the demand analysis procedure using the hybrid method of modeling. This method is preferred for a foundation constructed of a group of large-diameter CISS or CIDH shafts. Because of the large horizontal dimensions and substantial masses associated with the shafts in this type of foundation, the dynamic interaction of the shafts with the surrounding soil medium is more appropriately modeled and analyzed using the elastodynamic method; however, because the shafts resist loadings in a manner like piles, the local soil nonlinearities present in the soil–shaft interface regions near the ground surface where soft soils are usually present may be sufficiently large that they should be explicitly considered using a method such as the empirical *p–y* method.

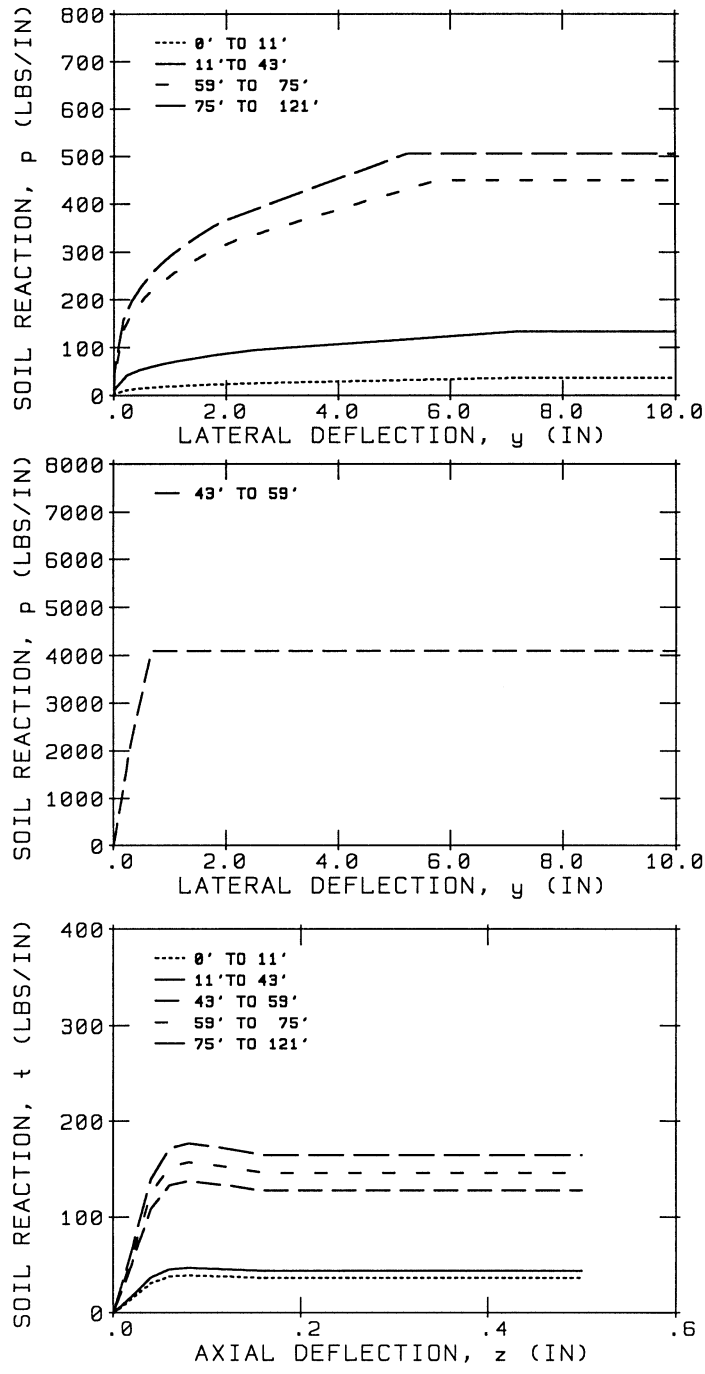

FIGURE 42.13 Typical *p–y* and *t–z* curves for the piles of the slender-pile group foundation considered.

The foundation selected for this example is composed of two 10.5-ft (3.2 m)-diameter shafts 150 ft (45.7 m) long, each consisting of a steel shell of wall thickness 1.375 in. (34.9 mm) filled with concrete. These two shafts are designed to be used as seismic retrofit shear piles for adding lateral stiffnesses and lateral load-resistance capacities to the H-pile group foundation considered in the second example discussed previously. The two shafts are to be linked to the existing pile group at

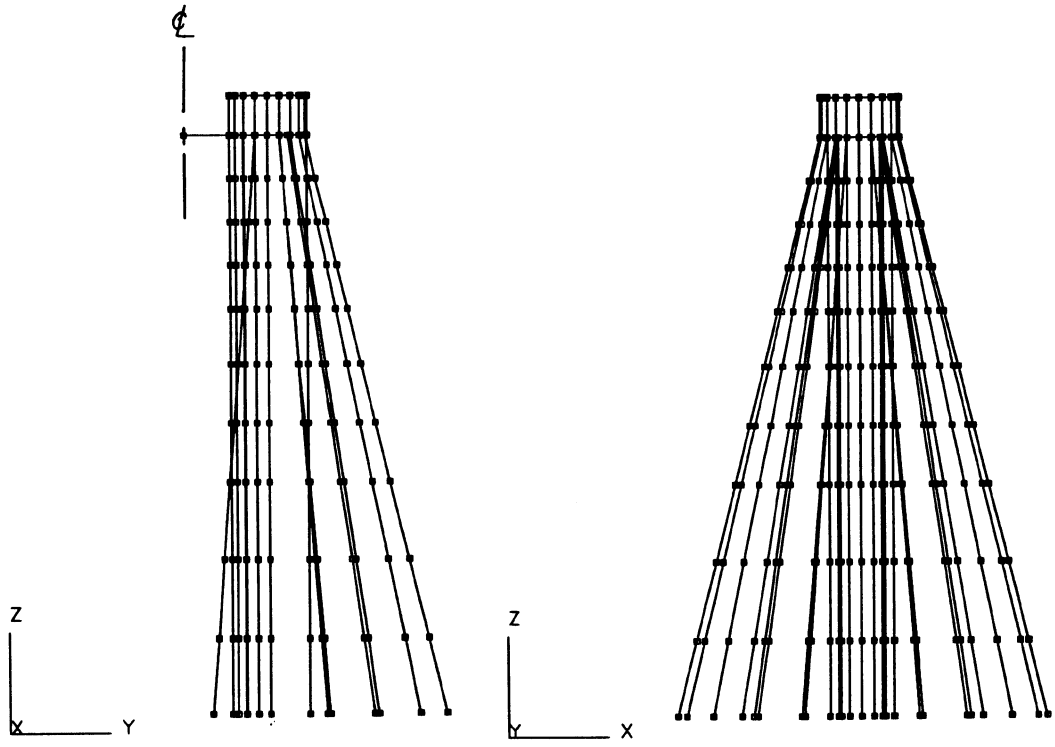

FIGURE 42.14 Beam-on-elastic-foundation half-model for the slender-pile group foundation considered.

the pile cap through a pile cap extension which permits the shafts to resist only horizontal shear loads acting on the pile cap, not axial loads and overturning moments. These shear piles have been designed to resist seismic horizontal shear loads acting on the pile head up to 3000 kips (13,344 kN) each.

To determine the foundation impedance matrix and the scattered pile cap motion vector associated with the horizontal displacements of the shafts at the pile cap, an SASSI model of one half of the soil–shaft system is developed, as shown in Figure 42.16. The soil properties used in this model are the strain-compatible properties shown in Table 42.1, which were obtained from the free-field site-response analyses using SHAKE; thus, the effects of global soil nonlinearities induced in the free-field soil by the design seismic input have been incorporated. To model the local soil nonlinearities occurring near the soil–shaft interface, three-directional (two lateral and one axial) soil springs are used to connect the beam elements representing the shafts to the soil nodes located at the boundary of the soil–shaft interfaces. The stiffnesses of these springs are derived in such a manner that they match the secant moduli of the empirical *p–y, t–z,* and *Q–d* curves developed for the shafts, as described previously in Section 42.5.3. Using the complete hybrid model shown in Figure 42.16, foundation compliances as functions of frequency were developed for harmonic pile-head shear loads varying from 500 (2224) to 3000 kips (13,334 kN). The results obtained are shown in Figure 42.17. It is seen that by incorporating local soil nonlinearities using the hybrid method, the resulting foundation compliance coefficients are not only frequency dependent due to the soil and shaft inertias and soil-layering effects as captured by the elastodynamic method, but they are also load–deflection amplitude dependent due to the local soil nonlinearities, as captured by the empirical *p–y* method. The shear load–deflection curves obtained at the pile head in the low-frequency range (≤1.0 Hz) are shown in Figure 42.18. The deflection curve for zero frequency, i.e., the static loading case, compares well with that obtained from a nonlinear analysis using LPILE f as indicated in Figure 42.18.

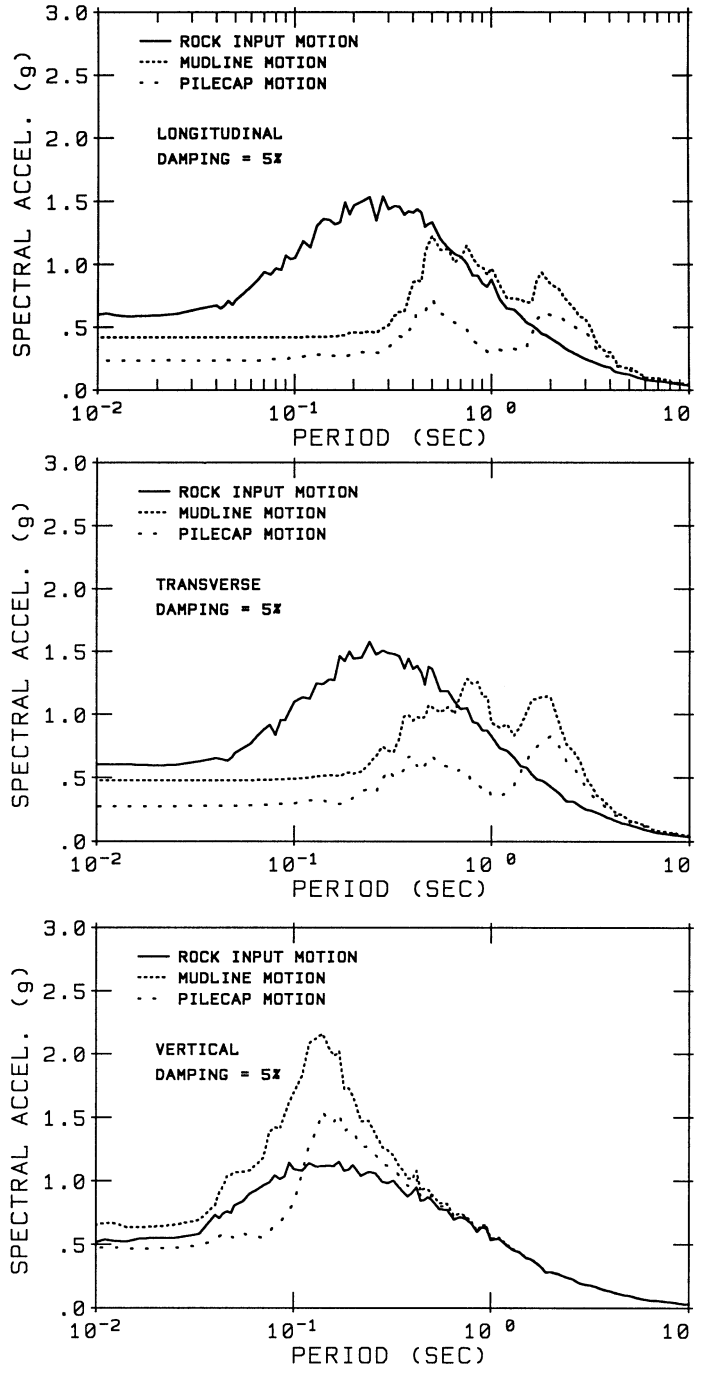

FIGURE 42.15 Comparisons of 5% damped response spectra for the rock input, mudline, and scattered pile cap motions in longitudinal, transverse, and vertical directions.

Subjecting the foundation to the design seismic input motions prescribed at the pile tip elevation and the corresponding free-field soil motions over its full depth, scattered foundation motions in the longitudinal and transverse directions of the bridge at the bottom center of the pile cap were

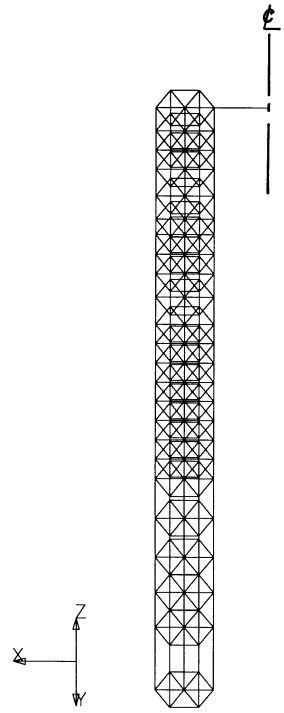

FIGURE 42.16 SASSI half-model of the large-diameter shaft foundation considered.

TABLE 42.1 Strain-Compatible Soil Properties for the Large-Diameter Shaft Foundation

El. ft (m)	Depth; ft (m)	Thickness; ft (m)	Unit Wt., $\frac{k}{ft^3}\left(\frac{kN}{m^3}\right)$	Shear Wave Velocity $\frac{ft}{s}\left(\frac{m}{s}\right)$	Shear Wave Damping Ratio	Compression Wave Velocity, $\frac{ft}{s}\left(\frac{m}{s}\right)$	Compression Wave Damping Ratio
–50 (–15.2)	0 (0.0)	10 (3.05)	0.096 (15.1)	202.1 (61.6)	0.10	4,800 (1,463)	0.09
–60 (–18.3)	10 (3.05)	10 (3.05)	0.096 (15.1)	207.5 (63.3)	0.15	5,000 (1,524)	0.10
–70 (–21.3)	20 (6.10)	10 (3.05)	0.096 (15.1)	217.7 (66.4)	0.17	5,000 (1,524)	0.10
–80 (–24.4)	30 (9.15)	20 (6.10)	0.110 (17.3)	137.5 (41.9)	0.25	4,300 (1,311)	0.10
–100 (–30.5)	50 (15.2)	10 (3.05)	0.096 (15.1)	215.7 (65.8)	0.20	4,800 (1,463)	0.10
–110 (–33.5)	60 (18.3)	20 (6.10)	0.096 (15.1)	218.4 (66.6)	0.20	4,300 (1,311)	0.10
–130 (–39.6)	80 (24.4)	20 (6.10)	0.096 (15.1)	233.0 (71.0)	0.20	4,900 (1,494)	0.10
–150 (–45.7)	100 (30.5)	20 (6.10)	0.120 (18.8)	420.4 (128.2)	0.20	5,500 (1,677)	0.10
–170 (–51.8)	120 (36.6)	10 (3.05)	0.120 (18.8)	501.0 (152.7)	0.19	6,000 (1,829)	0.10
–180 (–54.9)	130 (39.6)	10 (3.05)	0.120 (18.8)	532.7 (162.4)	0.19	5,800 (1,768)	0.10
–190 (–57.9)	140 (42.7)	20 (6.10)	0.125 (19.6)	607.2 (185.1)	0.18	5,800 (1,768)	0.10
–210 (–64.0)	160 (48.8)	20 (6.10)	0.128 (20.1)	806.9 (246.0)	0.16	5,800 (1,768)	0.10
–230 (–70.1)	180 (54.9)	10 (3.05)	0.133 (20.9)	1,374.4 (419.0)	0.11	6,400 (1,951)	0.10
–240 (–78.2)	190 (57.9)	5 (1.52)	0.140 (21.9)	2,844.9 (867.3)	0.02	12,000 (3,658)	0.02
–245 (–74.7)	195 (59.5)	halfspace	0.145 (22.8)	6,387.2 (1,947.3)	0.01	12,000 (3,658)	0.01

obtained as shown in terms of their 5% damped acceleration response spectra in Figure 42.19, where they can be compared with the corresponding response spectra for the seismic input motions and the free-field mudline motions. It is seen that, because of the substantial masses of the shafts, the spectral amplitudes of the scattered motions are higher than those of the free-field mudline motions

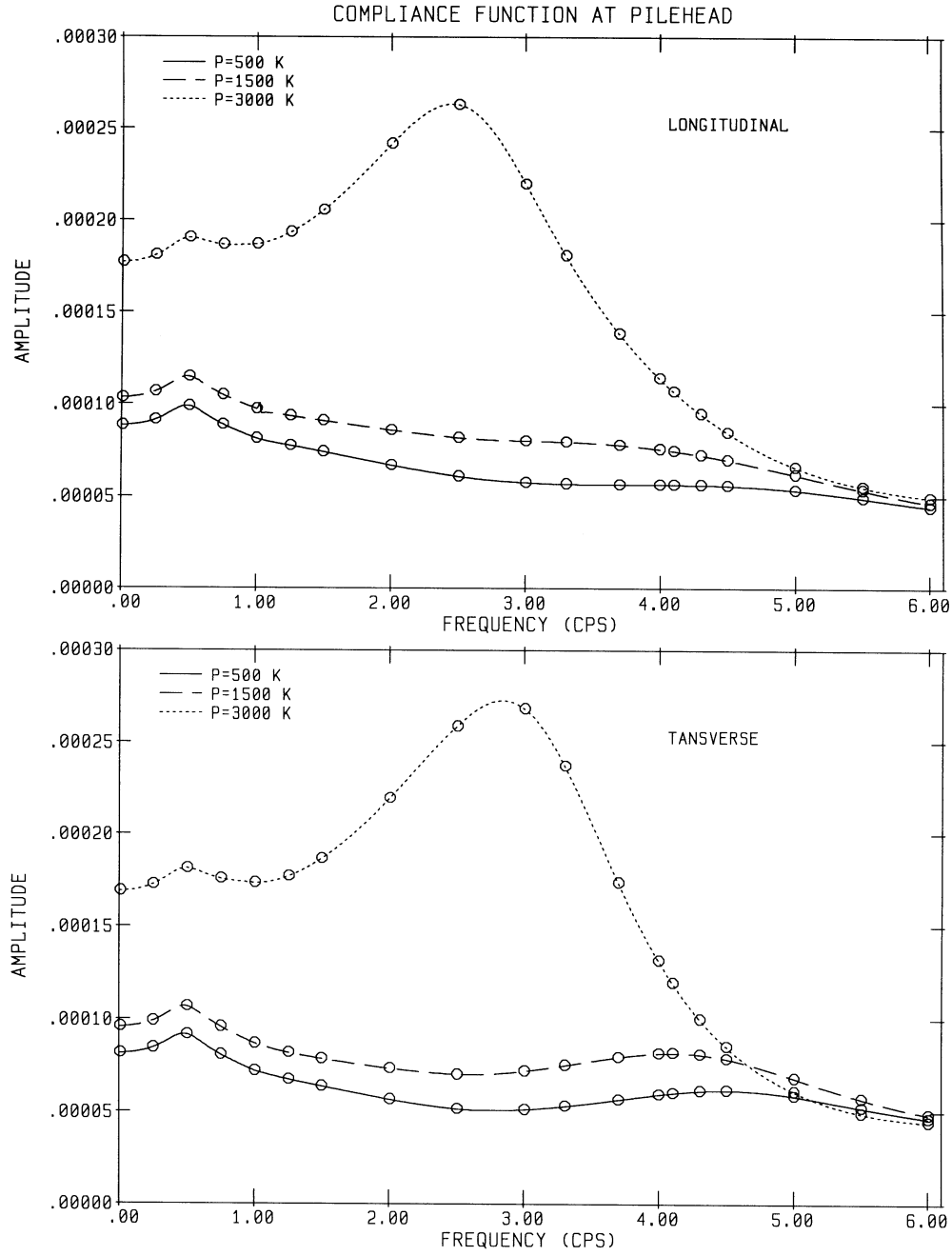

FIGURE 42.17 Foundation compliance functions at discrete values of shear load applied at the top of the shaft foundation.

for frequencies in the neighborhood of the soil–shaft system frequencies. Thus, for large-diameter shaft foundations constructed in deep, soft soil sites, it is important that the soil and shaft inertias be properly included in the SFI. Neglecting the shaft masses will result in underestimating the scattered pile cap motions in the longitudinal and transverse directions of the bridge, as represented in Figure 42.20.

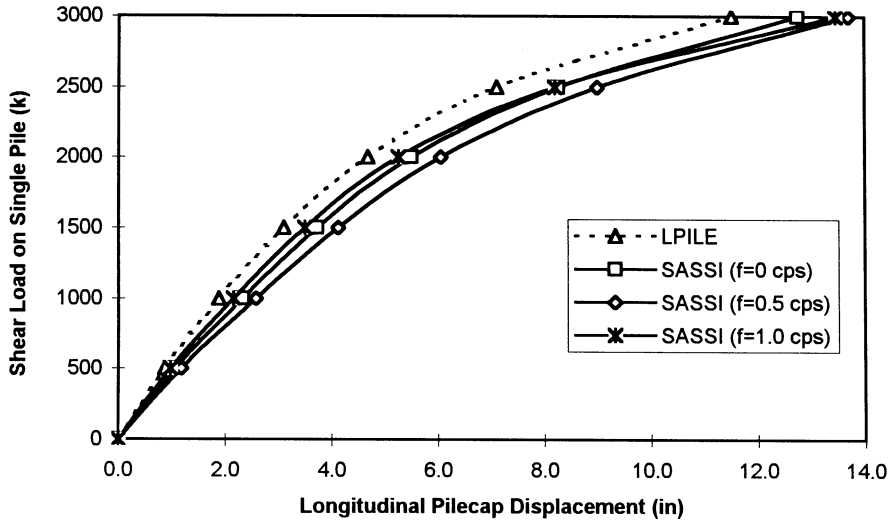

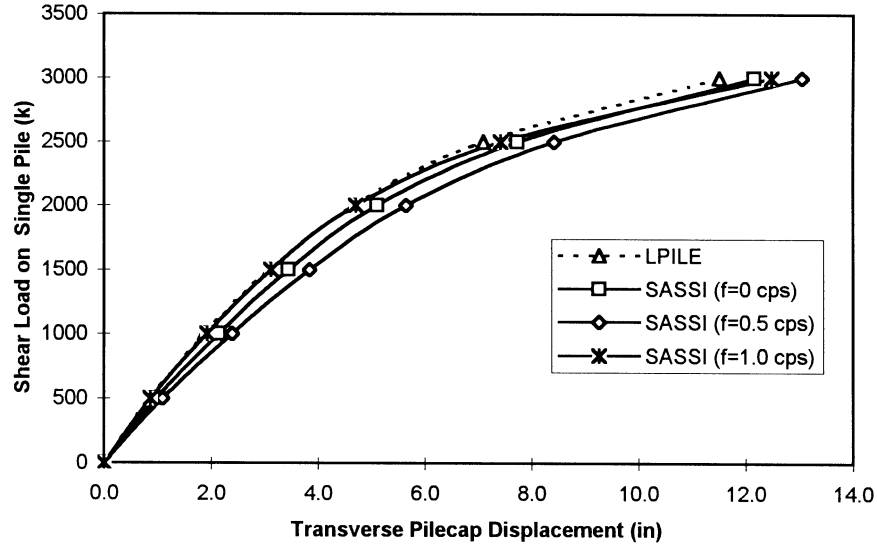

FIGURE 42.18 Typical sher load–deflection curves at several forcing frequencies.

42.8 Capacity Evaluations

The objective of the capacity evaluation is to determine the most probable levels of seismic resistance of the various elements, components, and subsystems of the bridge. The resistance capacities provided by this evaluation, along with the corresponding demands, provide the basis for judging seismic performance of the complete bridge system during future earthquakes. In the domain of SFSI as discussed here, the capacity evaluation focuses on soil–foundation systems.

For a bridge subjected to static loadings, the soil–foundation capacities of interest are the load resistances and the associated foundation deflections and settlements. Their evaluation constitutes the bulk of the traditional foundation design problem. When the bridge is subjected to oscillatory dynamic loadings, including seismic, the static capacities mentioned above are, alone, insufficient in the process of judging soil–foundation performance. In this case, it is necessary to assess the

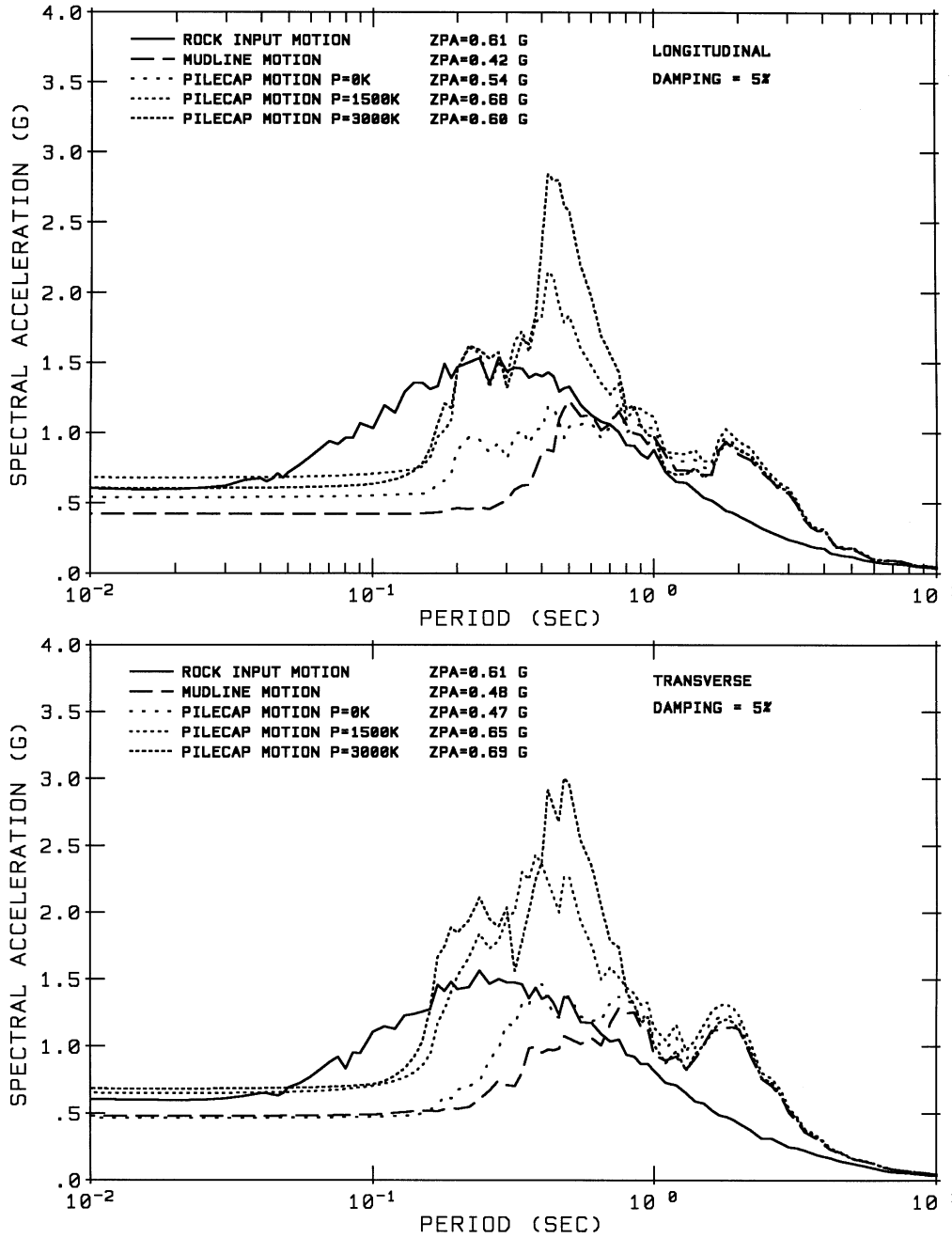

FIGURE 42.19 Comparisons of 5% damped response spectra for the longitudinal and transverse rock input, mudline, and scattered pile cap motions for the shaft foundations at several shear load levels.

entire load–deflection relationships, including their cyclic energy dissipation characteristics, up to load and/or deformation limits approaching failure conditions in the soil–foundation system. Because of the complexity of this assessment, the capacity evaluation must be simplified in order to make it practical. This is usually done by treating each soil–foundation system independently and by subjecting it to simplified pseudo-static monotonic and/or cyclic deformation-controlled step-by-step patterns of loading, referred to here as "push-over" analysis.

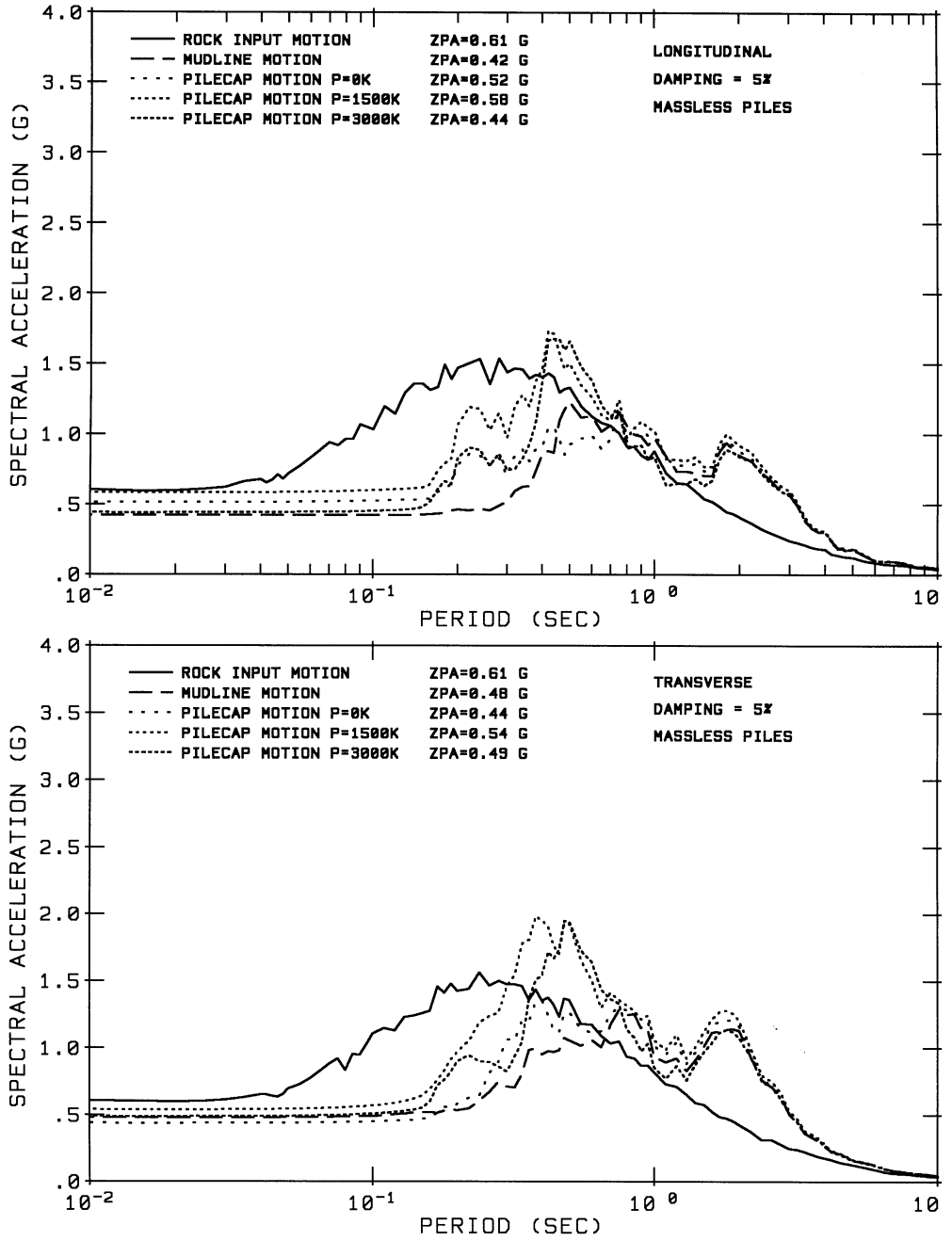

FIGURE 42.20 Comparisons of 5% damped response spectra for the longitudinal and transverse rock input, mudline, and scattered pile cap motions for the shaft foundation without masses in the shafts.

Because near-failure behavior of a soil–foundation system is involved in the capacity evaluation, it necessarily involves postelastic nonlinear behavior in the constituent components of the system, including the structural elements and connections of the foundation and its surrounding soil medium. Thus, ideally, a realistic evaluation of the capacities should be based on *in situ* tests conducted on prototypical foundation systems. Practical limitations, however, generally do not allow the conduct of such comprehensive tests. It is usually necessary, therefore, to rely solely on a

combination of analysis and limited-scope *in situ* or laboratory tests of selected critical components. These tests are performed either to provide the critical data needed for a capacity analysis or to confirm the adequacy and reliability of the results obtained from such an analysis. Indicator-pile tests that have often been performed for a bridge project are an example of limited-scope testing.

In a typical push-over analysis, the structural components of the foundation are represented by appropriate nonlinear finite elements capable of representing the near-failure nonlinear features, such as plastic hinging, ductile or brittle shearing, tensile or compressive yielding and fracturing, local and global buckling, and stiffness and capacity degradations due to P-Δ effects; further, the surrounding soil medium is usually represented either by nonlinear finite elements capable of modeling the postelastic constitutive behavior of the material or by empirically derived generalized nonlinear soil springs such as those developed from the p–y, t–z, and Q–d curves used for pile foundations. Ideally, the soil–foundation model used should also be able to represent properly the important nonlinear behaviors that could develop at the soil–foundation interfaces, such as slippage, debonding, and gapping. After the model has been developed, it is then subjected to a set of suitable push-over loading programs that simulate the loading conditions imposed on the soil–foundation system by the bridge pier at its interface with the foundation.

Conducting a step-by-step push-over analysis of the model described above, one can identify load and deformation levels associated with the various failure modes in the soil–foundation system. Then, load and deformation limits can be set beyond which the performance goals set for the bridge will no longer be met. These limits can be considered the capacity limits of the foundation system.

Because large uncertainties usually exist in a capacity evaluation, the capacity limits obtained therefrom should be reduced using appropriate capacity reduction ϕ factors. Each reduction factor adopted should adequately cover the lower limit of capacity resulting from the uncertainties. The reduced capacity limits established in this manner become the allowable capacity limits for use in comparing with the corresponding demands obtained through the demand analysis.

42.9 Concluding Statements

The previous sections of this chapter discuss the various elements of a modern state-of-the-art SFSI seismic analysis for large important bridges. These elements include (1) generating the site-specific rock-outcrop motions and corresponding free-field soil motions, (2) modeling and analysis of individual soil–foundation systems to establish foundation impedances and scattered motions, (3) determining SFSI using the substructuring method of analyses, and (4) assessing overall bridge performance by comparing force–deformation demands with corresponding capacities. Without retracing the details of these elements, certain points are worthy of special emphasis, as follows:

- Best-estimate rock and soil properties should be used in the generation of free-field seismic motions, with full recognition of the variations (randomness) and uncertainties (lack of knowledge) involved.
- Likewise, best-estimate material properties should be used in modeling the foundations, piers, abutments, and superstructure, also recognizing the variations and uncertainties involved.
- In view of the above-mentioned variations and uncertainties, sensitivity analyses should be conducted to provide a sound basis for judging overall seismic performance.
- Considering the current state of development, one should clearly differentiate between the requirements of a seismic force–deformation demand analysis and the corresponding capacity evaluation. The former is concerned with global system behavior; thus, it must satisfy only global dynamic equilibrium and compatibility. The latter, however, places emphasis on the behavior of local elements, components, and subsystems, requiring that equilibrium and compatibility be satisfied only at the local level within both the elastic and postelastic ranges of deformation.

- In conducting a demand analysis, equivalent linear modeling, coupled with the substructuring method of analysis, has the advantages that (1) the results are more controllable and predictable, (2) the uncertainties in system parameters can easily be evaluated separately, and (3) the SFSI responses can be assessed at stages. These advantages lead to a high level of confidence in the results when the nonlinearities are relatively weak. However, when strong nonlinearities are present, nonlinear time history analyses should be carried out in an iterative manner so that system response is consistent with the nonlinearities.
- When strong nonlinearities are present in the overall structural system, usually in the piers and superstructure, multiple sets of seismic inputs should be used separately in conducting the demand analyses; since, such nonlinearities cause relatively large dispersions of the maximum values of critical response.
- The elastodynamic method of treating SFSI is valid for foundations having large horizontal dimensions, such as large spread footings and caissons; while the empirical *p–y* method is valid only for slender-pile foundations subjected to large-amplitude deflections. For foundations intermediate between these two classes, e.g., those using large-diameter shafts, both of these methods are deficient in predicting SFSI behavior. In this case, the hybrid method of modeling has definitive advantages, including its ability to treat all classes of foundations with reasonable validity.
- The *p–y* method of treating SFSI in both demand analyses and capacity evaluations needs further development, refinement, and validation through test results, particularly with regard to establishing realistic *p–y*, t–z, and *Q–d* curves. For seismic applications, changes in the characteristics of these curves, due to global soil nonlinearities induced by the free-field ground motions, should be assessed.
- The hybrid method of treating SFSI, while being fundamentally sound, also needs further development, refinement, and test validation to make it fully acceptable for bridge applications.
- Systematic research and development efforts, involving laboratory and field tests and analytical correlation studies, are required to advance the SFSI analysis methodologies for treating bridge foundations.

The state of the art of SFSI analysis of large bridge structures has been rapidly changing in recent years, a trend that undoubtedly will continue on into the future. The reader is therefore encouraged to take note of new developments as they appear in future publications.

Acknowledgment

The authors wish to express their sincere thanks and appreciation to Joseph P. Nicoletti and Abbas Abghari for their contributions to Sections 42.2 and 42.4, respectively.

References

1. Mylonakis, G., Nikolaou, A., and Gazetas, G., Soil-pile-bridge seismic interaction: kinematic and inertia effects. Part I: Soft soil, *Earthquake Eng. Struct. Dyn.*, 26, 337–359, 1997.
2. Tseng, W. S., Soil-foundation-structure interaction analysis by the elasto-dynamic method, in *Proc. 4th Caltrans Seismic Research Workshop*, Sacramento, July 9–11, 1996.
3. Lam, I. P. and Law, H., Soil-foundation-structure interaction — analytical considerations by empirical *p–y* method, in *Proc. 4th Caltrans Seismic Research Workshop*, Sacramento, July 9–11, 1996.
4. Schnabel, P. B., Lysmer, J., and Seed, H. B., SHAKE — A Computer Program for Earthquake Response Analysis of Horizontally Layered Sites, Report No. EERC 72–12, Earthquake Engineering Research Center, University of California, Berkeley, 1972.

5. Tseng, W. S. and Hadjian, A. H., Guidelines for Soil-Structure Interaction Analysis, EPRI NP-7395, Electric Power Research Institute, Palo Alto, CA, October 1991.
6. Richart, F. E., Hall, J. R., Jr., and Woods, R. D., *Vibrations of Soils and Foundations*, Prentice-Hall, Englewood Cliffs, NJ, 1970.
7. Veletsos, A. S. and Wei, Y. T., Lateral and rocking vibration of footings, *J. Soil Mech. Found. Div. ASCE,* 97(SM9), 1227–1249, 1971.
8. Kausel, E. and Roësset, J. M., Soil-structure interaction problems for nuclear containment structures, in *Proc. ASCE Power Division Specialty Conference*, Denver, CO, August 1974.
9. Wong, H. L. and Luco, J. E., Dynamic response of rigid foundations of arbitrary shape, *Earthquake Eng. Struct. Dyn.*, 4, 587–597, 1976.
10. Seed, H. B. and Idriss, I. M., Soil Moduli and Damping Factors for Dynamic Response Analysis, Report No. EERC 70-10, Earthquake Engineering Research Center, University of California, Berkeley, 1970.
11. Waas, G., Analysis Method for Footing Vibrations through Layered Media, Ph.D. dissertation, University of California, Berkeley, 1972.
12. Lysmer, J., Udaka, T., Tsai, C. F., and Seed, H. B., FLUSH — A Computer Program for Approximate 3-D Analysis of Soil-Structure Interaction, Report No. EERC75-30, Earthquake Engineering Research Center, University of California, Berkeley, 1975.
13. Tang, Y. K., Proceedings: EPRI/NRC/TPC Workshop on Seismic Soil-Structure Interaction Analysis Techniques Using Data from Lotung Taiwan, EPRI NP-6154, Electric Power Research Institute, Palo Alto, CA, March 1989.
14. Matlock, H. and Reese, L. C., Foundation analysis of offshore pile supported structures, in *Proc. 5th Int. Conf. on Soil Mech. and Found. Eng.*, Paris, France, July 17–22, 1961.
15. Matlock, H., Correlations for design of laterally loaded piles in soft clay, in *Proc. Offshore Technology Conference,* Paper No. OTC1204, Dallas, TX, April 22–24, 1970.
16. Reese, L. C., Cox, W. R., and Koop, F. D., Analysis of laterally loaded piles in sand, in *Proc. Offshore Technology Conference,* Paper No. OTC2080, Dallas, TX, May 6–8, 1974.
17. Chang, C. Y., Tseng, W. S., Tang, Y. K., and Power, M. S., Variations of earthquake ground motions with depth and its effects on soil–structure interaction, *Proc. Second Department of Energy Natural Phenomena Hazards Mitigation Conference*, Knoxville, Tennessee, October 3–5, 1989.
18. Abrahamson, N. A., Spatial Variation of Earthquake Ground Motion for Application to Soil-Structure Interaction, Report No. TR-100463, Electric Power Research Institute, Palo Alto, CA, March 1992.
19. Gasparini, D. and Vanmarcke, E. H., SIMQKE: A program for Artificial Motion Generation, Department of Civil Engineering, Massachusetts Institute of Technology, Cambridge, 1976.
20. Silva, W. J. and Lee, K., WES RASCAL Code for Synthesizing Earthquake Ground Motions, State-of-the-Art for Assessing Earthquake Hazards in United States, Report 24, Army Engineers Waterway Experimental Station, Miscellaneous Paper 5-73-1, 1987.
21. Lilhanand, K. and Tseng, W. S., Development and application of realistic earthquake time histories compatible with multiple-damping design response spectra, in *Proc. 9th World Conference of Earthquake Engineers*, Tokyo-Kyoto, Japan, August 2–9, 1988.
22. Bolt, B. A. and Gregor, N. J., Synthesized Strong Ground Motions for the Seismic Condition Assessment of Eastern Portion of the San Francisco Bay Bridge, Report No. EERC 93-12, Earthquake Engineering Research Center, University of California, Berkeley, 1993.
23. Abrahamson, N. A., Nonstationary spectral matching, *Seismol. Res. Lett.*, 63(1), 1992.
24. Boore D. and Akinson, G., Stochastic prediction of ground motion and spectral response parameters at hard-rock sites in eastern North America, *Bull. Seismol. Soc. Am.*, 77, 440–467, 1987.
25. Sommerville, P. G. and Helmberger, D. V., Modeling earthquake ground motion at close distance, in *Proc. EPRI/Stanford/USGS Workshop on Modeling Earthquake Ground Motion at Close Distances*, August 23, 1990.

26. Papageorgiou, A. S. and Aki, K., A specific barrier model to the quantitative description of inhomogeneous faulting and the prediction of strong motion, *Bull. Seismol. Soc. Am.*, Vol. 73, 693–722, 953–978, 1983.
27. Bolt, B. A., Ed., *Seismic Strong Motion Synthetics*, Academic Press, New York, 1987.
28. U.S. Nuclear Regulatory Commission, *Standard Review Plan*, Section 3.71., Revision 2, Washington, D.C., August, 1989.
29. International Conference of Building Officials, *Uniform Building Code*, Whittier, CA, 1994.
30. Kaul, M. K., Spectrum-consistent time-history generation, *J. Eng. Mech. Div. ASCE,* 104(EM4), 781, 1978.
31. Penzien, J. and Watabe, M., Simulation of 3-dimensional earthquake ground motions, *J. Earthquake Eng. Struct. Dyn.*, 3(4), 1975.
32. Hao, H., Oliviera, C. S., and Penzien, J., Multiple-station ground motion processing and simulation based on SMART-1 array data, *Nuc. Eng. Des.*, III(6), 2229–2244, 1989.
33. Chang, C. Y., Power, M. S., Idriss, I. M., Sommerville, P. G., Silva, W., and Chen, P. C., Engineering Characterization of Ground Motion, Task II: Observation Data on Spatial Variations of Earthquake Ground Motion, NUREG/CR-3805, Vol. 3, U.S. Nuclear Regulatory Commission, Washington, D.C., 1986.
34. Abrahamson, N. A., Schneider, J. F., and Stepp, J. C., Empirical spatial coherency functions for application to soil-structure interaction analyses, *Earthquake Spectra*, 7, 1, 1991.
35. Tseng, W. S., Lilhanand, K., and Yang, M. S., Generation of multiple-station response-spectra-and-coherency-compatible earthquake ground motions for engineering applications, in *Proc. 12th Int. Conference on Struct. Mech. in Reactor Technology*, Paper No. K01/3, Stuttgart, Germany, August 15–20, 1993.
36. Vucetic, M. and Dobry, R., Effects of soil plasticity on cyclic response, *J. Geotech. Eng. ASCE,* 117(1), 89–107, 1991.
37. Sun, J. I., Golesorkhi, R., and Seed, H. B., Dynamic Moduli and Damping Ratios for Cohesive Soils, Report No. UBC/EERC-88/15, Earthquake Engineer Research Center, University of California, Berkeley, 1988.
38. Hardin, B. O. and Drnevich, V., Shear modulus and damping in soils: design equations and curves, *J. Soil Mech. Found. Div. ASCE,* 98(7), 667–691, 1972.
39. Seed, H. B., and Idriss, I. M., Soil Moduli and Damping Factors for Dynamic Response Analyses, Report No. EERC 70-10, Earthquake Engineering Research Center, University of California, Berkeley, 1970.
40. Seed, H. B., Wong, R. T., Idriss, I. M., and Tokimatsu, K., Moduli and Damping Factors for Dynamic Analyses of Cohesionless Soils, Report No. UCB/EERC-84/14, Earthquake Engineering Research Center, University of California, Berkeley, 1984.
41. Hardin, B. O. and Black, W. L., Vibration modulus of normally consolidated clay, *J. Soil Mech. Found. Div. ASCE,* 94(2), 353–369, 1968.
42. Hardin, B. O., The nature of stress-strain behavior for soils, *Proc. ASEC Geotech. Eng. Div. Specialty Conference on Earthquake Eng. and Soil Dyn.*, Vol. 1, 3-90, 1978.
43. Dickenson, S. E., Dynamic Response of Soft and Deep Cohesive Soils During the Loma Prieta earthquake of October 17, 1989, Ph.D. dissertation, University of California, Berkeley, 1994.
44. Idriss, I. M. and Sun, J. I., User's Manual for SHAKE 91, Center for Geotechnical Modeling, University of California, Davis, 1992.
45. Seed, H. B. and Idriss, I. M., Influence of soil conditions on ground motions during earthquakes, *J. Soil Mech. Found. Div.*, 95(SM1), 99–138, 1969.
46. Lee, M. K. W. and Finn, W. D. L., DESRA-2: Dynamic Effective Stress Response Analysis of Soil Deposits with Energy Transmitting Boundary Including Assessment of Liquification Potential, Report No. 38, Soil Mechanics Series, Department of Civil Engineering, University of British Columbia, Vancouver, 1978.

47. Prevost, J. H. DYNAFLOW: A Nonlinear Transient Finite Element Analysis Program, Department of Civil Engineering and Operations Research, Princeton University, Princeton, NJ, 1981; last update, 1993.
48. Prevost, J. H., DYNAID: A Computer Program for Nonlinear Seismic Site Response Analysis, Report No. NCEER-89-0025, National Center for Earthquake Engineering Research, Buffalo, New York, 1989.
49. Li, X. S., Wang, Z. L., and Shen, C. K., SUMDES, A Nonlinear Procedure for Response Analysis of Horizontally-Layered Sites, Subjected to Multi-directional Earthquake Loading, Department of Civil Engineering, University of California, Davis, 1992.
50. Apsel, R. J., Dynamic Green's Function for Layered Media and Applications to Boundary Value Problems, Ph.D. thesis, University of California, San Diego, 1979.
51. Lysmer, J., Tabatabaie-Raissai, M., Tajirian, F., Vahdani, S., and Ostadan, F., SASSI — A System for Analysis of Soil-Structure Interaction, Report No. UCB/GT/81-02, Department of Civil Engineering, University of California, Berkeley, 1981.
52. Reese, L. C., Awoshirka, K., Lam, P. H. F., and Wang, S. T., Documentation of Computer Program GROUP — Analysis of a Group of Piles Subjected to Axial and Lateral Loading, Ensoft, Inc., Austin, TX, 1990.
53. Reese, L. C. and Wang, S. T., Documentation of Computer Program LPILE — A Program for Analysis of Piles and Drilled Shafts under Lateral Loads," Ensoft, Inc., Austin, TX, 1989; latest update, Version 3.0, May 1997.
54. Reese, L. C. and Wang, S. T., Documentation of Computer Program APILE2 — Analysis of Load Vs. Settlement for an Axially Loaded Deep Foundation, Ensoft, Inc., Austin, TX, 1990.
55. Seed, H. B. and Idriss, I. M., Rock Motion Accelerograms for High-Magnitude Earthquakes, Report No. EERC 69-7, Earthquake Engineering Research Center, University of California, Berkeley, 1969.
56. Clough, R. W. and Penzien, J., *Dynamics of Structures,* 2nd ed., McGraw-Hill, New York, 1993.